
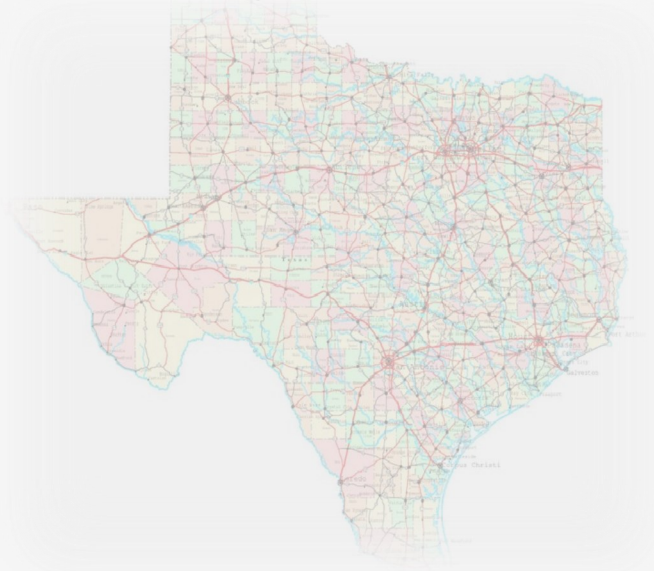




RESEARCH



**Effects of High Levels of
Obesity on Driver
Seat Belt Fit**



Effects of High Levels of Obesity on Driver Seat Belt Fit

Report #: ATLAS-2016-15

Monica L.H. Jones

Sheila M. Ebert

Matthew P. Reed

University of Michigan Transportation Research Institute



**University of Michigan
2901 Baxter Rd. Room 124
Ann Arbor, MI 48109-2150**

August 2016

DISCLAIMER

The contents of this report reflect the views of the authors, who are responsible for the facts and the accuracy of the information presented herein. This document is disseminated under the sponsorship of the U.S. Department of Transportation's University Transportation Centers Program, in the interest of information exchange. The U.S. Government assumes no liability for the contents or use there

ACKNOWLEDGMENTS

This research project was supported by the Center for Advancing Transportation Leadership and Safety (ATLAS Center). The ATLAS Center is supported by a grant from the U.S. Department of Transportation, Office of the Assistant Secretary for Research and Transportation, University Transportation Centers Program (DTRT13-G-UTC54). The ATLAS Center is a collaboration between the University of Michigan Transportation Research Institute (UMTRI) and the Texas A&M Transportation Institute (TTI).

The authors would like to thank Bruce Bradtmiller of Anthrotech who provided guidance on application of standard anthropometric techniques. Thanks to Dr. Oliver Varban of University of Michigan Adult Bariatric Surgery program who provided the opportunity to recruit participants for this study.

Laura Malik, Emily Lancaster and Rebecca Bubenheimer led the data collection. The team of students who assisted in data collection and data processing included Lisa Carver, Megan Bland, Riley Horn, Bansili Desai, Emma Yanakiev, Mac Morris, Lauren Eby, Swetha Reddi, Jamie Morrissey and Michelle Kearney.

We also thank Brian Eby and Brandon Waldron for construction of test fixtures.

Technical Report Documentation Page

1. Report No. ATLAS-2016-15	2. Government Accession No.	3. Recipient's Catalog No.	
4. Title and Subtitle Effects of High Levels of Obesity on Driver Seat Belt Fit		5. Report Date August 18, 2016	
		6. Performing Organization Code	
7. Author(s) Monica L.H. Jones, Sheila M. Ebert, Matthew P. Reed		8. Performing Organization Report No.	
9. Performing Organization Name and Address University of Michigan Transportation Research Institute (UMTRI) 2901 Baxter Road Ann Arbor, MI 48103		10. Work Unit no. (TRAIS)	
		11. Contract or Grant No. DTRT13-G-UTC54	
12. Sponsoring Agency Name and Address Advancing Transportation Leadership and Safety (ATLAS) Center 2901 Baxter Rd., Room 124, Ann Arbor, MI 48109-2150 U.S.A		13. Type of Report and Period Covered	
		14. Sponsoring Agency Code	
15. Supplementary Notes Supported by a grant from the US Department of Transportation, OST-R, University Transportation Centers Program			
16. Abstract Obesity has been shown to increase the risks to motor vehicle occupants of some types of injury in crashes. The effects of obesity on injuries are not well understood and current prevention efforts do not effectively address the vulnerability associated with the high body mass index (BMI) cohort. Previous studies demonstrated that obesity effectively introduces slack in the seat belt restraint system by routing the belt further away from the underlying skeletal structures. These studies, however, have not measured individuals with a BMI ≥ 40 kg/m ² . Because approximately 5% of US adults have BMI exceeding this threshold, this study extends the previous research on the relationships between body habitus and belt fit with data from 52 male and female licensed drivers with BMI from 31 to 59 kg/m ² (median 38 kg/m ²). Consistent with previous research, higher BMI was associated with a lap belt position further forward and higher relative to the pelvis. On average, a person with a BMI of 40 places the belt 118 mm above and 68 mm forward of the anterior-superior iliac spine landmarks on the pelvis. Previous studies have shown mean values of 31 mm and 33 mm, respectively, for individuals with BMI 25. The data suggest a continued focus on improving restraint systems for individuals with high BMI is needed.			
17. Key Words Vehicle Occupant Safety, Safety Belts, Belt Fit, Obesity, Posture		18. Distribution Statement Unlimited	
19. Security Classification (of this report) Unclassified	20. Security Classification (of this page) Unclassified	21. No. of Pages 84	22. Price

CONTENTS

ACKNOWLEDGMENTS	2
INTRODUCTION	5
METHODS	6
RESULTS.....	24
DISCUSSION	44
CONCLUSIONS.....	47
REFERENCES	48
APPENDIX A. Scripted Instructions	50
APPENDIX B. Standard Anthropometry.....	52
APPENDIX C. Whole-Body Scanning.....	59
APPENDIX D. Individual Belt Fit	80

INTRODUCTION

Several studies have found that obesity is associated with increased risk of severe-to-fatal injury for vehicle occupants in crashes (Zhu et al., 2006; Viano et al., 2008; Sivak et al., 2010; Jehle et al., 2012). Using data from detailed crash investigations, Rupp et al. (2013) modeled the effects of obesity on the risks of injury to different body regions for different crash types. Increasing body mass index (BMI) was associated with an increase in the risk of AIS 3+ lower extremity and spine injuries in frontal crashes, and an increased risk of upper extremity injury in frontal and nearside crashes. In a study that modeled the relative effects of age, gender, and BMI on the number of occupants with serious-to-fatal injury, the effect of BMI was largest on frontal crashes with an increased risk of lower extremity injuries, and on nearside crashes with an increased risk of thorax injuries (Carter et al., 2014). These results demonstrate a need to improve understanding of the occupant protection needs of individuals with high BMI.

Obese occupants are at increased risk for severe injury due to anatomical and physiological variations that alter normal occupant and safety belt response during a crash (Zhu et al. 2006; Turkovich and van Roosmalen, 2010). An increase in forward hip and knee excursion has been observed for obese cadavers during sled crash tests (Kent et al. 2010) and simulation studies (Turkovich et al., 2013). Greater occupant mass increases kinetic energy that must be managed, and soft tissue in the abdomen area changes belt routing and contributes to increased excursion in frontal crashes. Reed et al. (2013) demonstrated that higher BMI is associated with poor lap belt fit, with the lap portion of the belt riding higher and more forward relative to the pelvis and an associated increase in lap belt webbing length. Both of these factors are associated with poorer belt performance in frontal impacts.

Approximately 72 million adults, 34% of the US adult population, are obese (Flegal et al., 2010) with a BMI greater than or equal to 30 kg/m². Currently about 5% of US adults are “morbidly” obese, defined by the CDC (1998) as a BMI ≥ 40 kg/m². This cohort has increased at a faster rate among adults in the US than is the prevalence of moderate obesity (Sturm, 2007). In the United States, the growth rate in the prevalence of a BMI >40 kg/m² and a BMI >50 kg/m² has been found to be twice and three times, respectively, the growth rate of the prevalence of moderate obesity since 2000 (Sturm, 2007). The issue of disproportionate increases in the more extreme categories of BMI is important because the adverse health risks amplify as the level of obesity increases (Pasco et al., 2013).

As the prevalence of severe obesity increases, the protection of obese occupants will become increasingly important in vehicle and restraint design. Previous studies that investigated the effects of obesity on belt fit have not measured individuals with a BMI ≥ 40 kg/m² (Reed et al., 2012; Reed et al., 2013). The current study extends the previous research on the relationships between body habitus and belt fit to BMI ≥ 40 kg/m².

METHODS

Participants

This study included twenty-six women and twenty-six men (total N=52). Participants were stratified based on BMI, stature, and age. The CDC typically subdivides obesity into the following categories: Class I: BMI of 30 – 34.9 kg/m², Class II: BMI of 35 – 39.9 kg/m², Class III: BMI ≥ 40 kg/m². Class III obesity is sometimes categorized as “extreme” or “severe” obesity (CDC, 1998). Figure 1 shows the size distribution of the participants, and Figures 2-3 show the range of body shapes captured in the study. Tables 1-3 list the overall body dimensions of the study participants.

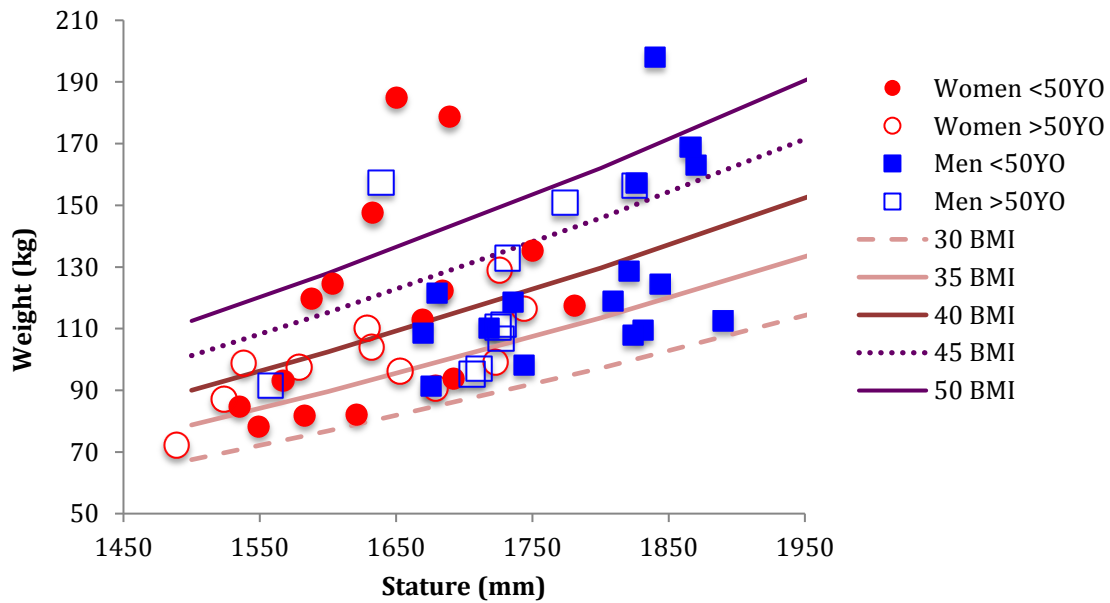


Figure 1. Weight versus stature of participants.

Table 1. Canonical and Standing Dimensions.

Measurements (<i>mm unless noted</i>)	Percentiles								
	Min	Max	Mean	5th	25th	50th	75th	95th	
Stature (without shoes)	1489	1890	1698	1537	1631	1699	1756	1854	
Weight (kg)	72	198	117	82	97	111	129	173	
BMI (kg/m ²)	31	68	41	32	33	38	44	59	
Age at Testing (yr)	21	73	47	24	34	47	59	70	
Standing									
Chest Depth Scapula	215	442	328	233	308	323	359	392	
Chest Depth Spine	204	385	281	219	264	284	304	326	
Waist Depth	218	520	353	251	313	347	391	484	
Stance Breadth	31	525	348	233	300	347	392	487	
Foot Breadth	81	112	98	87	94	98	103	109	
Chest Circumference (Axilla)	992	1490	1207	1033	1135	1187	1266	1448	
Chest Circumference (Bust Pt.)	1029	1505	1255	1089	1137	1260	1341	1469	
Waist Circumference (Max Lat.)	204	1623	1230	990	1111	1238	1356	1545	
Waist Circumference (Max Ant.)	941	1845	1265	1030	1123	1225	1361	1648	
Hip Circ. (Max Post.)	825	1960	1278	1042	1148	1233	1387	1652	
Waist Circumference (Omph.)	890	1715	1250	985	1116	1204	1380	1583	
Upper Thigh Circumference	479	1054	711	585	661	711	737	861	
Max Anterior Protrusion Height	800	1504	1010	869	930	1007	1069	1209	
Max Posterior Protrusion Height	761	1504	914	789	842	871	938	1231	
Omphalion Height	794	1495	978	829	904	966	1024	1169	

Table 2. Seated Dimensions.

Measurements (<i>mm unless noted</i>)	Min	Max	Mean	Percentiles				
				5th	25th	50th	75th	95th
Seated								
Erect Sitting Height	789	992	890	801	859	892	922	973
Eye Height (Sitting)	683	876	780	691	750	779	811	858
Acromial Height (Sitting)	522	677	606	534	572	608	641	670
Knee Height	470	693	541	484	516	540	563	601
Tragion to Top of Head	110	141	127	117	123	127	129	138
Head Length	176	218	199	186	194	199	206	213
Head Breadth	143	170	158	147	155	157	163	167
Shoulder-Elbow Length	283	409	359	309	340	363	382	397
Elbow-Hand Length	340	543	467	408	452	474	490	521
Buttock-Knee Length 1*	579	750	656	601	622	653	687	723
Buttock-Knee Length 2**	563	795	660	602	628	655	681	726
Buttock-Popliteal Length 1*	479	642	551	499	523	552	577	607
Buttock-Popliteal Length 2**	458	645	550	499	527	549	580	606
Neck Breadth	13	170	128	109	120	128	137	156
Bideltoid Breadth	327	748	549	473	511	538	584	659
Biacromial Breadth	309	486	402	357	375	398	429	459
Forearm-Forearm Breadth	467	791	611	514	574	606	638	737
Waist Breadth (Max)	349	626	433	354	390	423	463	554
Hip Breadth (Max)	378	650	474	398	437	464	503	583
Knee-Knee Breadth 1 *	292	646	414	311	363	400	453	567
Knee-Knee Breadth 2 **	296	694	495	348	427	504	534	673
Hand Breadth	71	108	88	73	83	90	93	100
BiASIS Breadth	203	333	236	208	224	233	244	271
Neck Circumference	335	641	451	365	410	455	481	549
Upper Arm Circumference	330	615	402	334	365	395	425	492
Axilla to Cubital Fold	132	516	177	140	160	170	183	207
Calf Circumference	351	680	459	382	427	450	478	559
Ankle Circumference	199	432	258	206	237	252	273	314

*legs held as close to parallel to midsagittal plane as possible, ** legs started as close to parallel as possible, then natural splay allowed

Table 3. Supine Dimensions.

Measurements (<i>mm unless noted</i>)	Min	Max	Mean	Percentiles				
				5th	25th	50th	75th	95th
Supine								
Abdominal Extension Max	228	406	305	243	270	292	330	393
Midline-Elbow Breadth	327	490	401	347	370	393	428	472
Waist Breadth (Max)	348	598	433	359	395	420	470	550
Hip Breadth (Max)	375	680	481	404	437	478	499	587
Knee-Knee Breadth	261	577	417	300	387	418	460	520
Thigh Breadth Right	173	320	228	182	208	222	244	281
Thigh Breadth Left	159	284	220	180	204	214	237	271
Calf Breadth Right	108	225	144	118	133	141	155	176
Calf Breadth Left	109	210	144	114	132	140	154	182
Waist Circumference (Omph.)	908	1640	1215	973	1089	1193	1298	1544

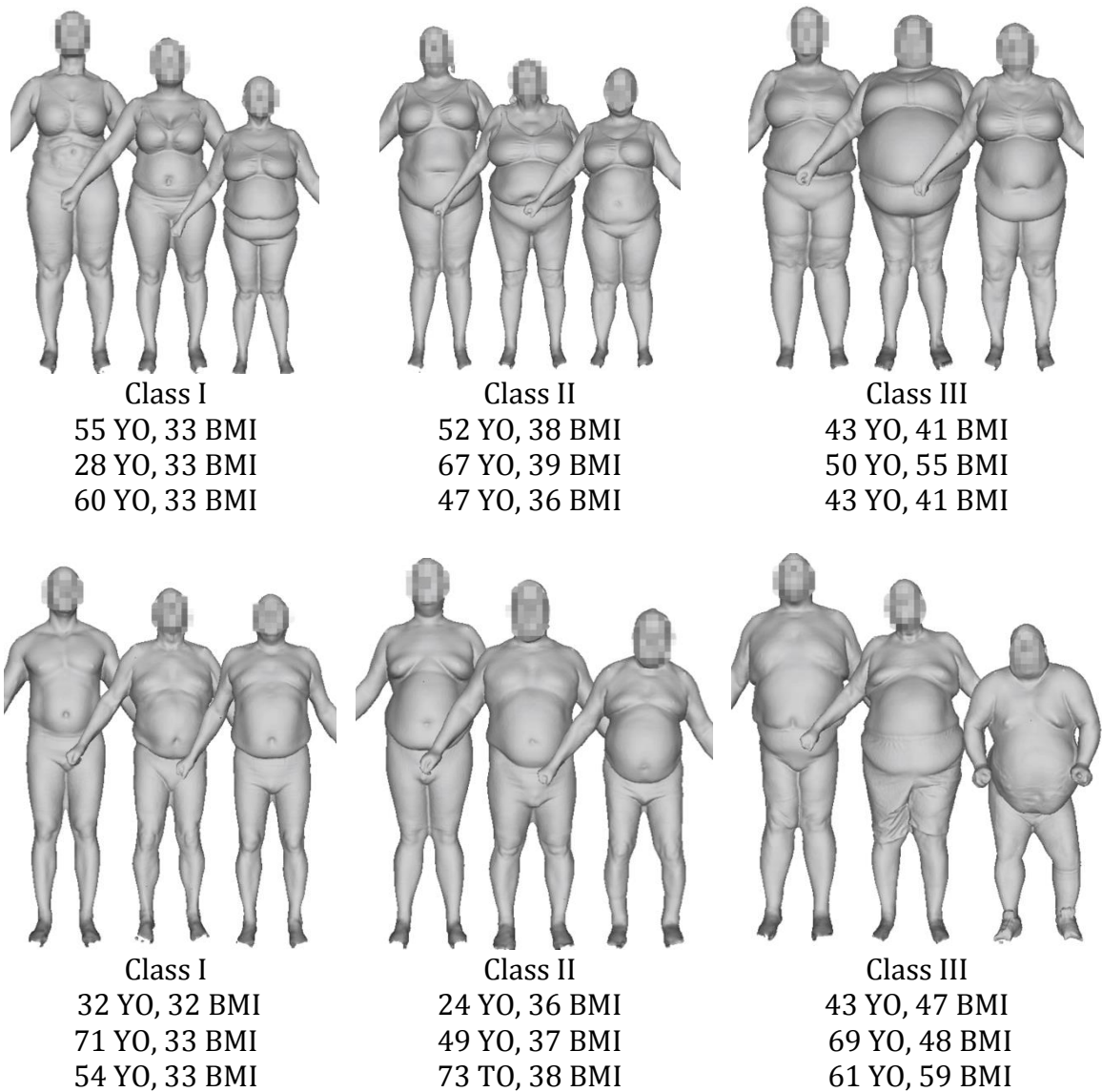


Figure 2. Examples of participants across the range of BMI in standing posture by CDC obesity class (CDC, 1998).

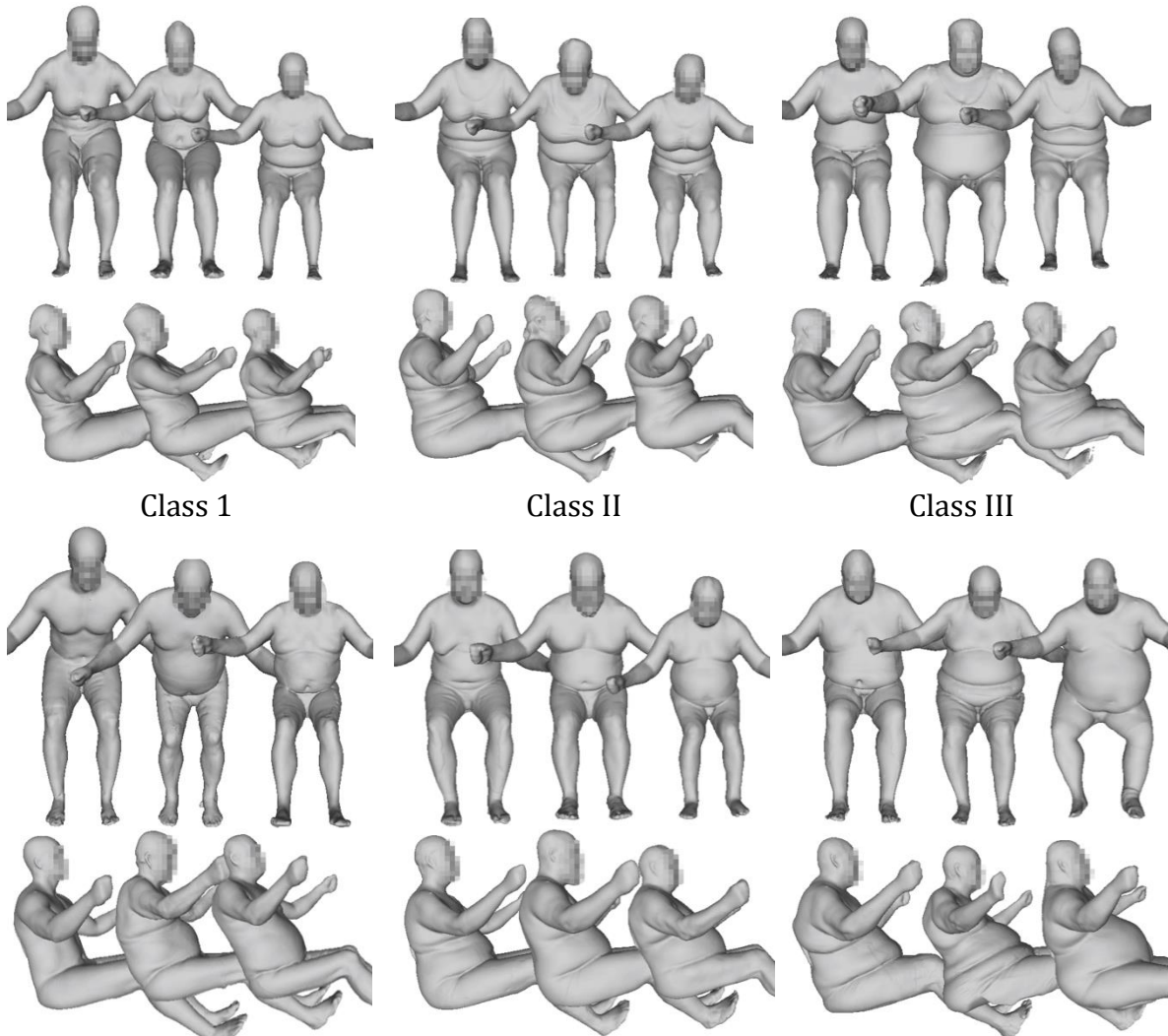


Figure 3. Examples of participants across the range of BMI in driving posture.

Protocol Approval

The study protocol was approved by the University of Michigan Institutional Review Board (IRB) for Health Behavior and Health Sciences (IRB #HUM00102426). Participants were recruited through online postings and through healthcare providers at the University of Michigan Adult Bariatric Surgery program. Each participant was briefed on the purposes and methods of the study and written consent was obtained. All testing was completed in a single session of about three hours.

Measurement Protocol in Mockup

A driver workstation mockup used in previous studies (Reed et al. 2013) was modified for use in the current testing (Figure 4). The driver mockup included a tilting steering wheel, instrument panel, brake and accelerator pedals, six-way power seat, and seat belt. The relationships between the seat, steering wheel, and pedals were adjustable to represent a wide range of different vehicle packages. The driver mockup was equipped with a six-way power seat with a power recline adjuster and a large range of vertical adjustment. The seat was mounted on a motorized platform that could be moved fore-aft so that all participants were able to select a comfortable seat position without being censored by the available seat track adjustment range.

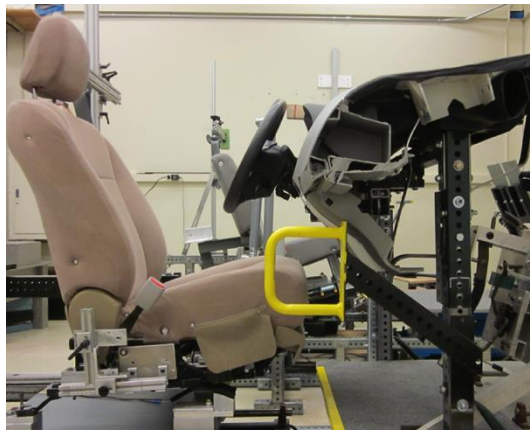


Figure 4. Driver mockup.

The vehicle packages chosen as test conditions listed in Table 4 and illustrated in Figures 5 and 6 were among those used in several previous UMTRI studies and are designed to span a large percentage of passenger car, light truck, minivan, and SUV packages. Conditions were distinguished by values of steering wheel fore-aft position (SAE L6 or L11), steering wheel height above the heel surface (SAE H17), and seat height (SAE H30). The pedal plane angle was also changed according to SAE J1516 for each seat height. The steering wheel angle was varied at each seat height. Seat back and cushion angles were initially set to 23° relative to vertical and 14.5° relative to horizontal, respectively (SAE J826). In the vehicle mockup the orientation of the right-handed coordinate system followed SAE J1100 with +X pointing rearward parallel to the long axis of the mockup, +Y pointing to the passenger/inboard side of the mockup, and +Z pointing up.

Table 4. Driver Mockup Package Geometry.
 (Color-coded represents package configuration in Figure 5)

Package Condition Number	H-point			Steering Wheel			Pedal	
	Z	X relative to AHP		X		Z	Angle (deg.)	Angle (deg.)
	H30	Male	Female	L11	L6	H17		
D1	180	902	755	584	649	578	23°	71°
D2*		882	735	534	599			
D3		861	714	484	549			
D4*	270	833	679	507	601	646	25°	62°
D5		905	850	457	551			
D6*		902	755	407	501			
D7	360	882	735	425	550	715	27°	51°
D8*		861	714	375	500			
D9		833	679	325	450			

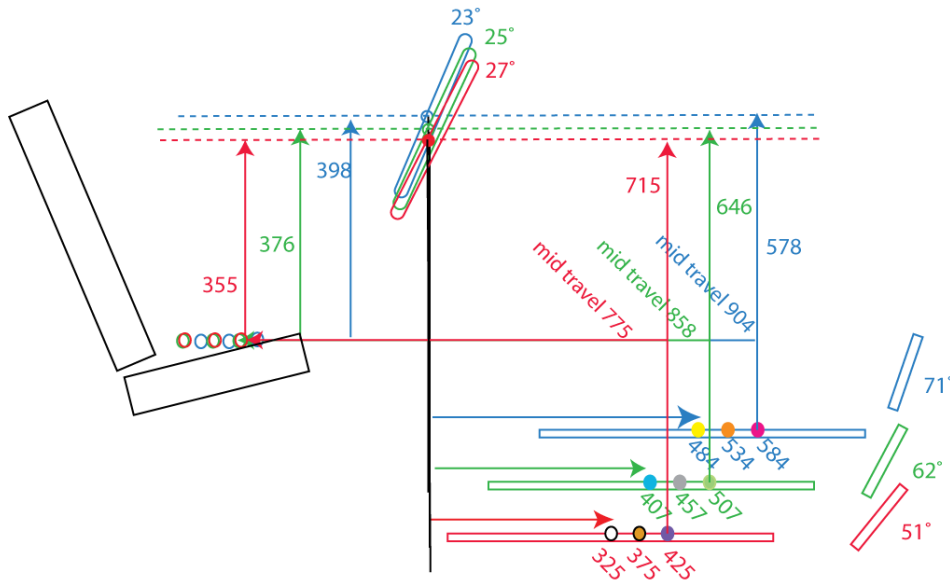


Figure 5. Illustration of driver mockup packages.
 (Color-coded represents package configuration in Table 4)

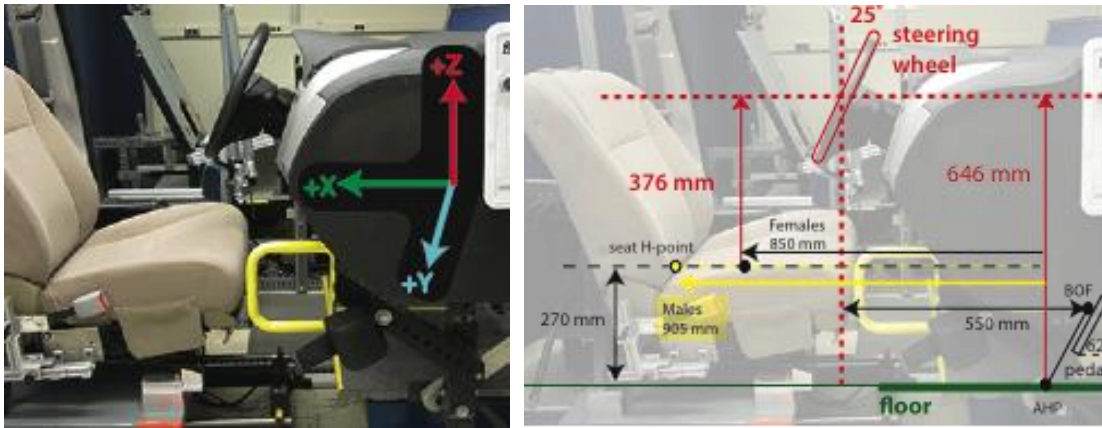


Figure 6. Package dimensions of vehicle mockup for mid condition (D5). Fore-aft and up-down H-point locations are starting positions; participants were able to adjust the seat fore-aft and up-down position, and the seat back and seat cushion angle to their preferred posture.

The driver mockup was equipped with a three-point seatbelt with a sliding latch plate. The retractor and D-ring were mounted to a fixture allowing the D-ring location to be adjusted over a wide range. With the D-ring at its typical position, the lower anchorages were adjusted to present the flattest and steepest belt angles permitted under FMVSS 213 (30° and 75°). Five belt configurations were obtained by manipulating the belt anchorage locations. Table 5 lists the conditions. Because previous work showed that the D-ring location had minimal effect on lap belt fit across a range of lap belt angles, the effects of D-ring location and lap belt angle were examined separately, each at three levels. The shoulder belt YZ and XZ angles were manipulated together, creating three D-ring locations: one location high, rearward, and inboard; one location low, forward, and outboard; and one midrange location. Figures X and X illustrate the belt configurations. The lap belt angles were set relative to seating reference point (SgRP) and were equivalent on the inboard (buckle) and outboard sides.

Table 5. Driver Mockup Package Geometry.

Condition Number		Shoulder Belt		Lap Belt		
Package	Belt	ZX Angle (deg)	YZ Angle (deg)	XZ Angle (deg)		
D1	DB1	26°	21°	52°		
D2*						
D3						
D4*						
D7						
D8*						
D9						
D5	DB1	26°	21°	52°		
	DB2			30°		
	DB3			75°		
	DB4			24.5°	17°	52°
	DB5			31.0°	24°	

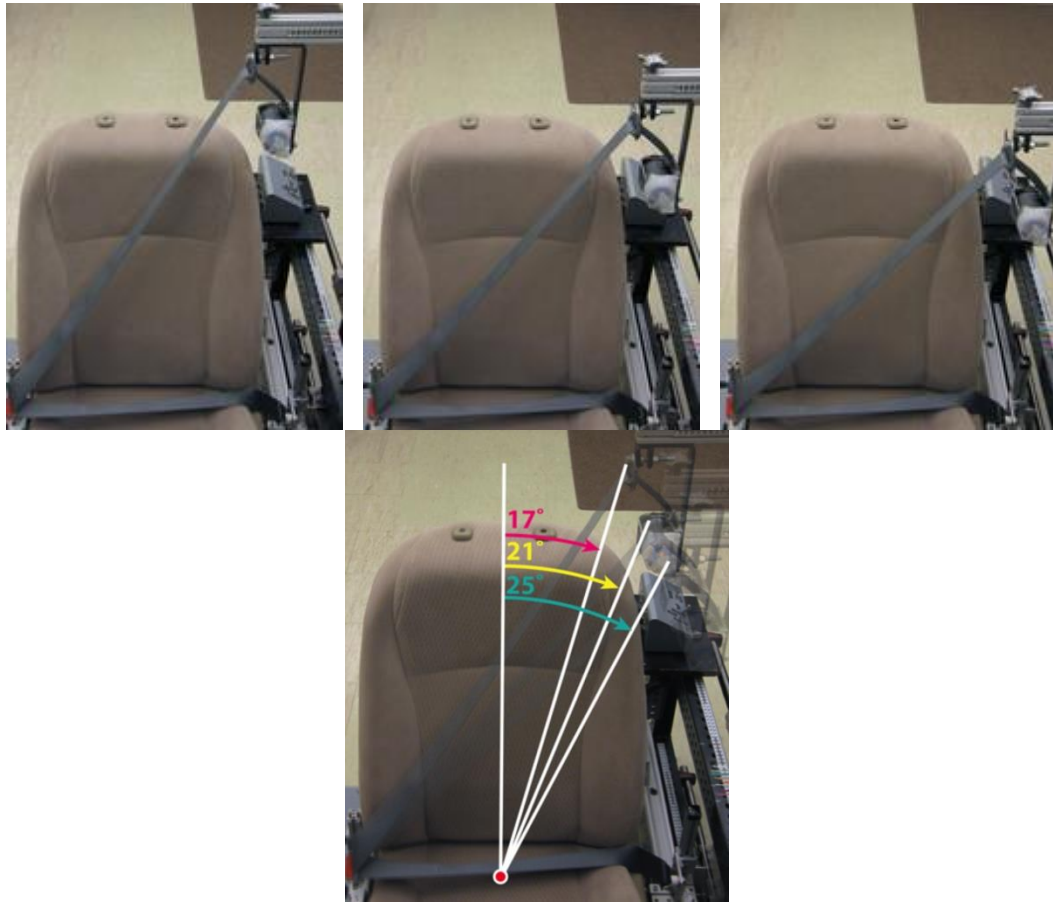


Figure 7. Illustration of shoulder belt conditions with (left to right) YZ angles of 17, 21, and 25 degrees.

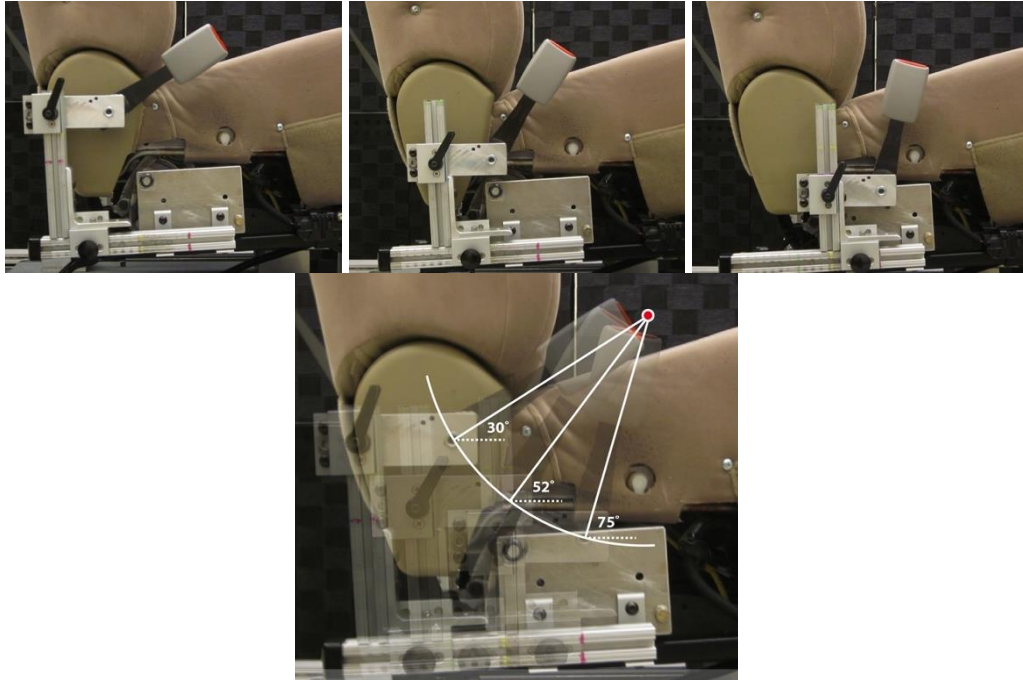


Figure 8. Lap belt buckle anchorage locations for belt fit conditions at 30, 52, and 75 degrees to horizontal.

While seated in the driving mockup, the participant was trained in the operation of each seat adjuster and demonstrated use of the components for the investigator. The initial positions of each participant-adjustable component were set to the same midrange values prior to each trial. The participant entered the mockup and adjusted the seat (fore-aft position, vertical position, cushion angle, backrest angle) to obtain a comfortable driving posture. The participant then donned the belt and assumed a normal driving posture.

The investigator used the FARO Arm coordinate digitizer to record the three-dimensional locations of landmarks on the participant's body and on the mockup, seat, and belt (Table 6). In addition, a stream of points with approximately 5 mm spacing was recorded along the edges of lap and shoulder portions of the belt between the anchorages and latch plate (Figure 8).

Due to the difficulty of locating the ASIS points on obese participants, the investigator used the tool in Figure 9 to assist in digitizing the ASIS points in the vehicle mockup. The distance between the ASIS points (bispinous breadth) measured with a caliper anthropometer away from the mockup where the investigator had better access to the lap area. With the breadth marked on the tool, the tool was centered on the lap of the participant. The investigator then began palpating the abdomen at these locations and then firmly deflected the flesh over the ASIS while digitizing (Figure 10).

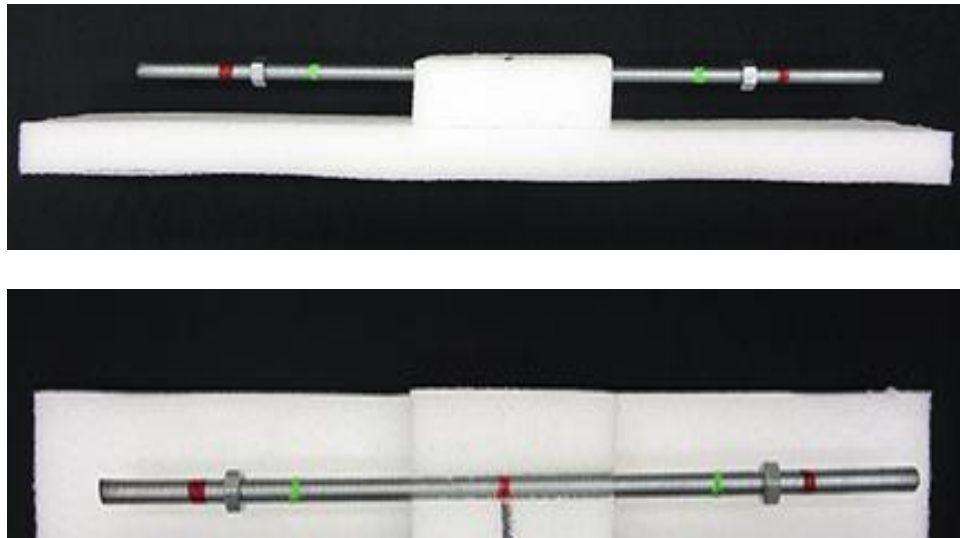


Figure 9. Tool used to aid in finding the ASIS points in the vehicle mockup. The locations of the nuts on the threaded rod were adjusted to the participants bispinous (bi-ASIS) breadth recorded during standard anthropometry.



Figure 10. Palpating a participant's ASIS using the tool to locate the ASIS points in the driver mockup.

Table 6. Points Recorded on Participant and Vehicle Mockup.

	<u>Mockup</u>
<u>Participant</u>	Accelerator Pedal
C7 (Cervicale)	Floor
Back Of Head (Max Rearward)	Steering Wheel Center
Top Of Head (Max Height)	
Tragion Lt	<u>Seat</u>
Ectoorbitale Lt	Measured before and after participant's adjustments
Infraorbitale at Pupil Center Lt	3 Points on Seat Cushion (references tracking up-down, fore-aft and tilt)
Glabella	2 Points on Seat Back (references tracking recline angle)
Suprasternale	
Substernale	
Medial Clavicle Lt	
Lateral Clavicle Lt	<u>Restraint System</u>
Anterior of Acromion Lt	D-ring Reference Point
Lateral Humeral Epicondyle Lt	Lower Anchorage Reference Point
Ulnar Styloid Process, Lateral Lt	Buckle Reference Point
ASIS Lt and Rt	
Suprapatella Lt and Rt	Shoulder Belt:
Infrapatellat Lt	Inboard and Outboard Edge on Clavicle
Lateral Femoral Epicondyle Lt	Top and Bottom Edge at Participant's Midline
Medal Femoral Epicondyle Rt	Inboard Edge at Participant's Suprasternale Height
Toe (Bottom edge of sole, longest shoe point) Lt	
Ball of Foot Lateral Lt	Lap Belt:
Ball of Foot Medial Rt	Top Edge and Bottom edge at ASIS lateral position (Lt & Rt) and at Participant's Midline
Heel (Bottom edge of sole at midline) Lt & Rt	
Lateral Malleolus Lt	
Medial Malleolus Rt	

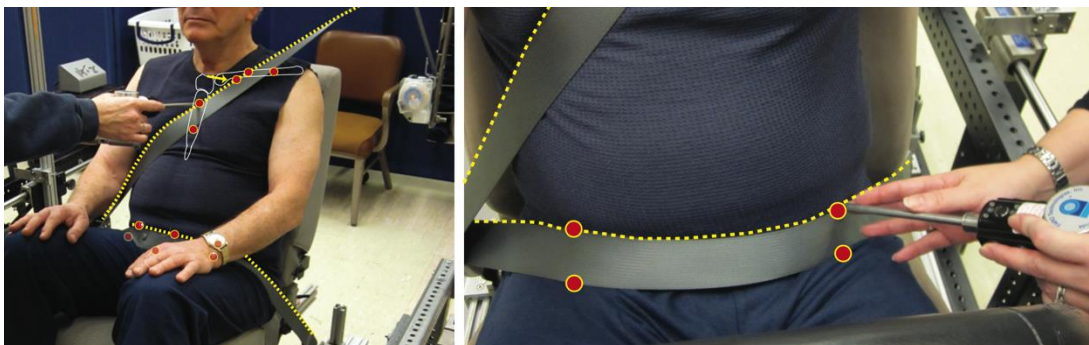


Figure 11. Continuous streams of point data (dashed line) were collected along the entire length of the webbing in addition to point data (red circles). Both the shoulder and lap belt were recorded along the upper edge of the webbing.

Traditional Anthropometry

Standard anthropometric dimensions, including stature, body weight, and linear breadths and depths were gathered from each participant to characterize the overall body size and shape, following the procedures in Hotzman et al. (2009). All measurements were obtained from the participants in minimally clad test clothing. Subsets of the anthropometric measures were obtained at multiple measurement site(s) to provide preliminary data on points of maximal breadth, depth, or girth. The intention of these maximal measures was to capture body shape variability, particularly the location and contour of the panniculus during standing, supine, and seated postures. Measurements were added to better quantify the range and the postural effects of obesity. Additions include measuring participants with a natural leg splay in addition to legs parallel and in supine postures. Table 7 contains a complete list of measurements. All measurements were obtained minimally clad, except that stature was measured with and without footwear to characterize shoe heel height. Figure 12 shows examples of the measurements taken with the participant in a supine position. Appendix B describes the measurement procedures for those measures unique to this study.

Table 7. Standard and Adapted Anthropometric Dimensions.

<u>Sitting</u>	<u>Standing</u>
Erect Sitting Height	Stature**
Eye Height (Sitting)	Chest Depth Scapula
Acromial Height (Sitting)	Chest Depth Spine
Tragion to Top of Head	Waist Depth
Knee Height	Foot Length
Head Length**	Foot Breadth
Head Breadth**	Stance Breadth**
Shoulder-Elbow Length	Circumference at Axilla
Elbow-Hand Length	Circumference at Bust Point
Neck Breadth **	Circumference at Maximum Lateral Protrusion **
Bideltoid Breadth**	Circumference at Maximum Anterior Protrusion **
Biacromial Breadth	Circumference at Maximum Posterior Protrusion **
Forearm-Forearm Breadth **	Circumference at Omphalion
Waist Breadth (Max)†	Upper Thigh Circumference
Hip Breadth (Max) †	Height of Maximum Anterior Protrusion
Hand Breadth**	Height of Maximum Posterior Protrusion
BiASIS Breadth (Bispinous)	Height of Omphalion**
Neck Circumference**	Weight**
Upper Arm Circumference**	
Axilla to Cubital Fold**	
Calf Circumference**	
Ankle Circumference	
	<u>Supine</u>
	Abdomen Extension Depth†
<u>With thighs parallel and natural leg splay</u>	Front Chest Midline-Elbow Breadth†
Buttock-Knee Length**	Waist Breadth (Max) †
Buttock-Popliteal Length**	Hip Breadth (Max) †
Knee-Knee Breadth**	Knee-Knee Breadth**
	Thigh Breadth Right & Left**
	Calf Breadth Right & Left**
	Waist Circ. (Omphalion)

** same as Anthrotech, † difference from Anthrotech (not 30° table) and max widths at both hip and waist

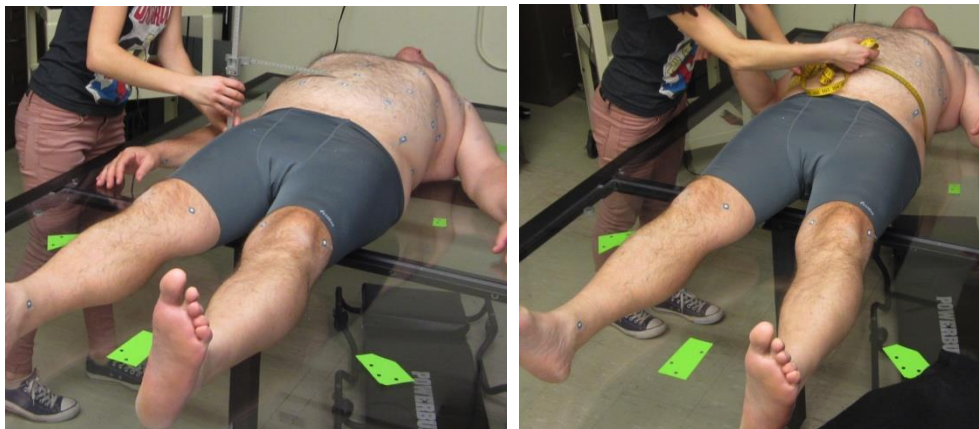


Figure 12. Investigator measuring a participant in supine posture.

Hardseat

Body landmark locations were recorded in the laboratory hardseat shown in Figure 13. The hardseat allows access to posterior spine and pelvis landmarks that are inaccessible in the automotive seat. The hardseat has a 14.5° “cushion” (pan) angle and a 23° back angle designed to produce postures similar to those in an automotive seat. Table 8 lists the landmarks recorded in the hardseat.



Figure 13. Hardseat.

Table 8. Hardseat Landmarks and Scanning Markers.

Back of Head	Lateral Femoral Epicondyle Rt and Rt	C7
Top Of Head (Vertex)	Lateral Femoral Epicondyle Marker Lt and Rt	C7 Marker
Tragion Rt and Rt	Lateral Fibular Head Lt and Rt	T4
Ectoorbitale Lt and Rt	Medial Femoral Epicondyle Lt and Rt	T4 Marker
Infraorbitale at Pupil Center Lt and Rt	Medial Femoral Epicondyle Marker Lt and Rt	T8
Glabella	Medial Tibial Condyle Rt	T8 Marker
Medial Clavicle Lt and Rt	Suprapatella Lt and Rt	T12
Lateral Clavicle Lt and Rt	Infrapatella Lt and Rt	T12 Marker
Acromion Lt and Rt (Anterior)	Heel Lt and Rt	L1
Acromion Lt Marker	Malleolus Lateral Lt and Rt	L1 Marker
Humeral Epicondyle Lateral Lt and Rt	Lateral Ankle Marker Lt and Rt	L2
Lateral Elbow Lt Marker	Ball of Foot Lateral Lt and Rt	L2 Marker
Humeral Epicondyle Medial Lt and Rt	Toe (Longest Tibiale) Lt and Rt	L3
Medial Elbow Lt Marker	Ball of Foot Medial Lt and Rt	L3 Marker
Ulnar Styloid Process Lt and Rt	Malleolus Medial Lt and Rt	L4
Radial Styloid Process Lt and Rt	Medial Ankle Rt Marker	L4 Marker
Wrist Mid Top Marker Lt and Rt	Rib10 Marker Lt and Rt	L5
Wrist Mid Bottom Marker Lt and Rt	Lateral Torso Ctr Marker Lt and Rt	L5 Marker
Lateral Hand Lt and Rt	Iliocristale Marker Lt and Rt	ASIS Lt and Rt
Medial Hand Lt and Rt	Torso Mid Top Marker Lt and Rt	PSIS Lt and Rt
Suprasternale	Torso Mid Bot Marker Lt and Rt	
Substernale		
Chest Triad Markers (3)		
Acromion Rt (Anterior)		
Acromion Rt Marker		

Analysis: Quantifying Belt Fit

Lap belt fit was quantified by the fore-aft and vertical location of the upper/rearward margin of the lap portion of the belt at the lateral location of the anterior-superior iliac spine (ASIS) landmarks on the left and right sides of the pelvis (Figures 14 and 15). This was in accordance with previous belt fit studies (Reed et al. 2012, Reed et al. 2013). The correction for adiposity at the ASIS landmarks documented in Reed et al. (2013) was used. Shoulder belt fit was quantified by the lateral location of the inboard edge of the shoulder portion of the belt relative to the body midline at the height of the suprasternale landmarks (Figure 16). The Y-axis (medial lateral) distance between the body midline and belt is termed shoulder belt score (Reed et al. 2009, Reed et al. 2012, Reed et al. 2013). A fifth-order Bézier curve was fit to the lap and shoulder belt stream points to smooth measurement error. The amount of belt feed out was calculated by finding the lengths of the lap belt between the lower outboard anchor and the buckle, and the shoulder belt between the D-ring and buckle were calculated along the Bézier curve.

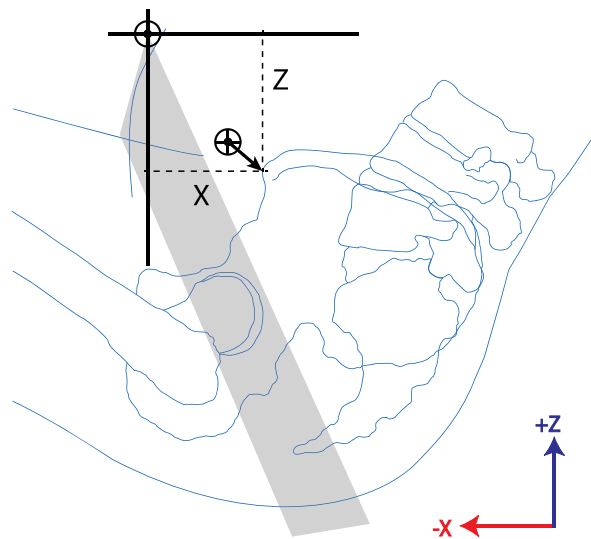


Figure 14. Locations of points recorded on the lap belt.

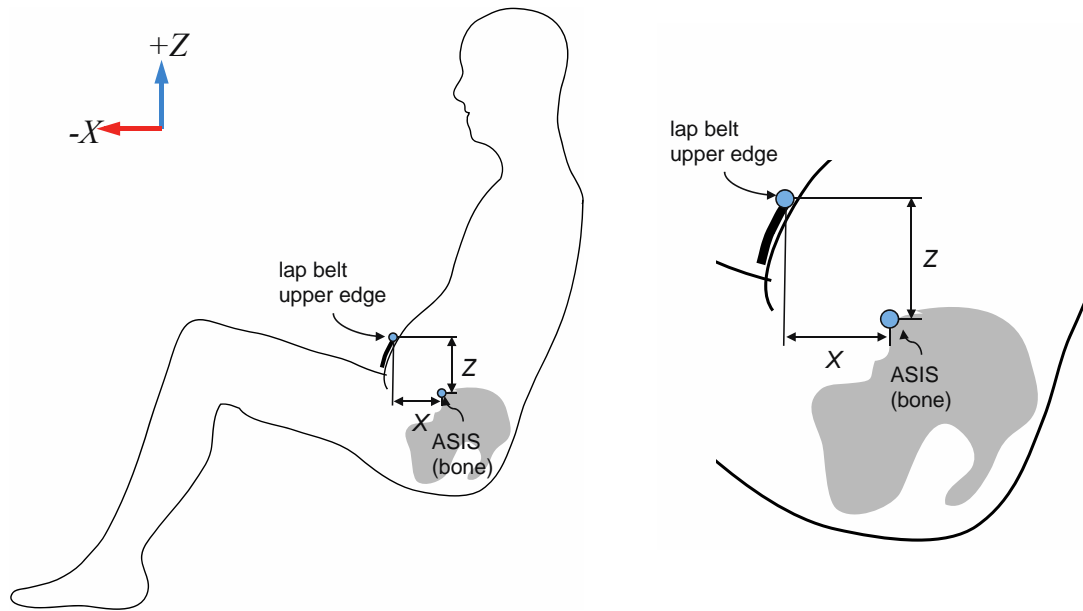


Figure 15. Dependent measures for lap belt fit. The upper/rearward edge of the lap portion of the belt is measured at the lateral position of the right and left predicted ASIS location. The fore-aft (X) coordinate is positive rearward of the ASIS and the vertical coordinate is positive above the ASIS landmark.

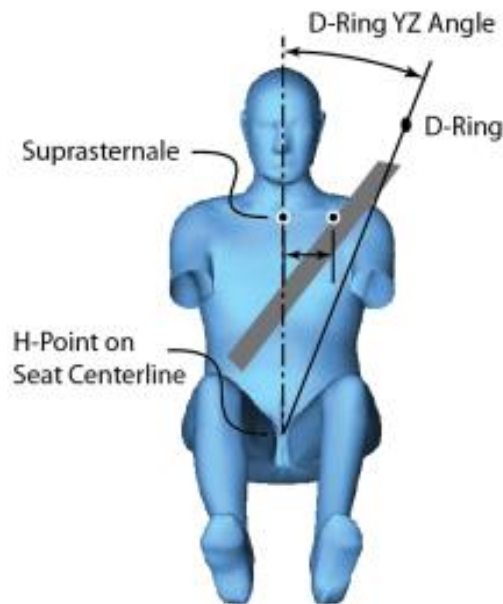


Figure 16. Torso (shoulder) belt fit measurement. Larger positive values indicate more outboard belt placement. The definition of D-ring YZ Angle is also shown.

Statistical Analysis

Regression analysis was used to determine relationships between X and Z lap belt scores and lengths with anthropometric, lap belt angle, and seat position variables and to assess potential nonlinearities. Lap belt angle and seat position variables, stature, body mass index (BMI), age, gender, and two-way interactions were considered as potential predictors. In an effort to obtain a more parsimonious model an interactive procedure was followed, whereby variables contributing less than 0.02 to the adjusted R-value were removed. All terms, and each model, are statistically significant with $p < 0.01$. The importance of the regression function terms was evaluated by multiplying each coefficient by the range of the independent measure that is present in the data. Analysis of variance (ANOVA) and post hoc contrast tests were used to evaluate significant effects. A conservative P-value of 0.0001 was used to determine the statistical significance of the effects in the ANOVA. An alpha level of 0.05 was adopted for all post hoc Tukey tests.

RESULTS

Lap Belt Fit

Three lap belt trials were included in the analysis of the X and Z lap belt scores for each participant (DB1, DB2, and DB3). Because driver-selected seat position affects the lap belt angle associated with the outboard (vehicle-mounted) anchorage, an effective lap belt angle (ELBA) was used in this analysis (Reed et al. 2013). ELBA was computed as the side-view angle from the outboard belt anchorage to the seat H-point in the position selected by the participant. This is in contrast to the standard measure of lap belt angle used in FMVSS 210, which defines lap belt angle with respect to a particular H-point location. Seat position was quantified as the fore-aft position of the seat H-point relative to the ball-of-foot reference point (X) and accelerator heel point (Z) (see SAE J1100).

Figure 17 illustrates the distribution of the LapBeltX and LapBeltZ scores. The overall mean (SD) of the lap belt scores for 52 male and female licensed drivers with BMI from 31 to 59 kg/m² (median 38 kg/m²) was -91 (51) mm for LapBeltX and 62 (24) mm for LapBeltZ.

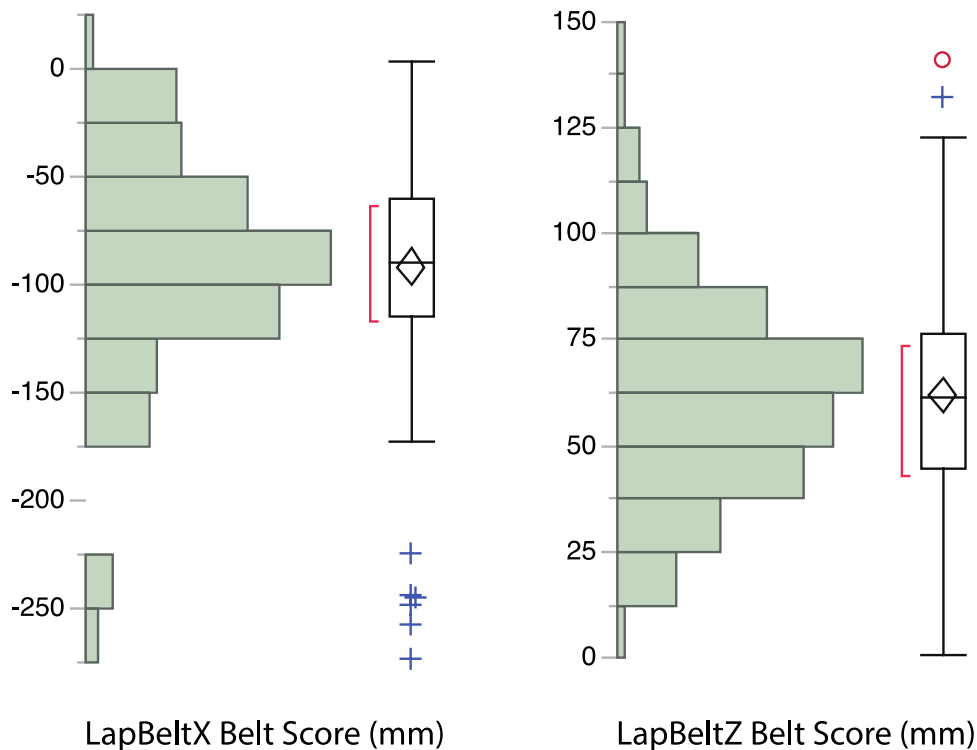


Figure 17. Distribution of the LapBeltX and LapBeltZ scores. Box plots show the median and interquartile range (IQR); whiskers indicate the maximum or minimum values within 1.5 IQR in distance from the nearest quartile of the LapBeltX and LapBeltZ.

Figure 18 shows the lap belt location with respect to ASIS for male and female participants for all trials. On average, the upper edge of the lap belt was an additional 32 mm forward of the ASIS landmark on the pelvis with each higher level of obesity classification.

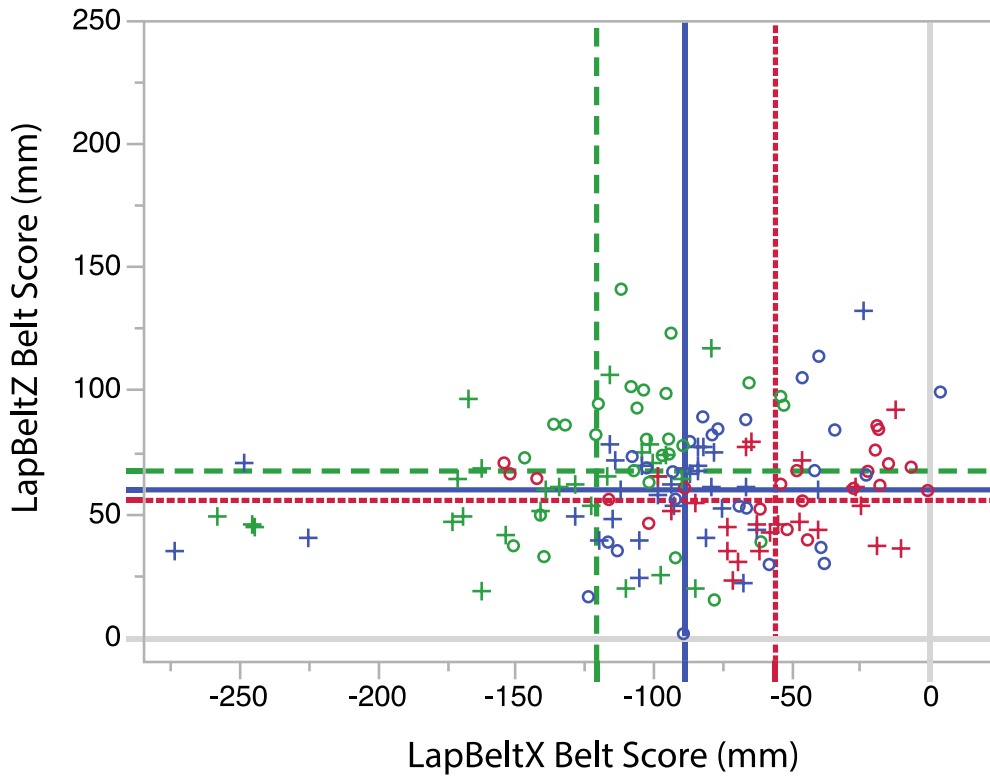


Figure 18. Lap belt location for all trials for women (o) and men (+). Data are coded based upon a participant's BMI classification: class 1 (red, - - - -), class II (blue, ———), and class III (green, - - - -). The lines indicate the mean values of lap belt fit X and Z scores for each BMI classification: X=-56mm, Z=56mm for Class I, X=-89mm, Z=60mm for Class II, and X=-121mm, Z=68mm for Class III.

LapBeltX

In the regression analysis, BMI was the most important determinant of LapBeltX. Note that lower values (more negative) indicate that the belt is farther from the pelvis. Table 9 shows a regression model that indicates that LapBeltX was also affected by gender and stature. Interactions between the participant covariates were tested but not found to be significant. The adjusted R^2 for this model is 0.36; the adjusted R^2 for a model with BMI only is 0.33.

Table 9. Regression model predicting LapBeltX. (mm, $R^2_{adj} = 0.40$, RMSE=39.6)

Term	Estimate	Std Error	t Ratio	Prob> t
Intercept	79.08	19.38	4.08	<.0001*
Gender[F]	18.56	4.18	4.44	<.0001*
BMI	-4.30	0.48	-8.99	<.0001*
Gender[F]:(Stature - 1698.84)	0.13	0.06	2.20	0.0292*
Gender[M]:(Stature -1698.84)	0.15	0.06	2.72	0.0073*

The importance of each of the predictors on LapBeltX was evaluated by multiplying the estimated effect by the range of the variable in the data. The range of BMI is 31.3 to 58.6 kg/m², which resulted in a mean difference of 114 mm in position of the horizontal placement of the lap belt relative to the ASIS across the same range. A BMI value of 10 kg/m² higher was associated with a lap belt position 43 mm farther forward relative to ASIS. Gender had a smaller effect that was not accounted for by the stature difference between men and women. On average a 24 mm difference in the fore-aft location of the lap belt was observed between female and male participants after accounting for stature and BMI. Lap belt angle and age did not have significant effects on LapBeltX.

Median LapBeltX values associated with Class I, II, and III obesity are summarized in Figure 19. Significant differences were observed between LapBeltX positions for participants between each level of BMI classification. Figure 20 also shows bivariate plots of the fore-aft lap belt location stratified by BMI classification and gender. LapBeltX varied significantly for female and male participants classified as Class I and Class II obesity.

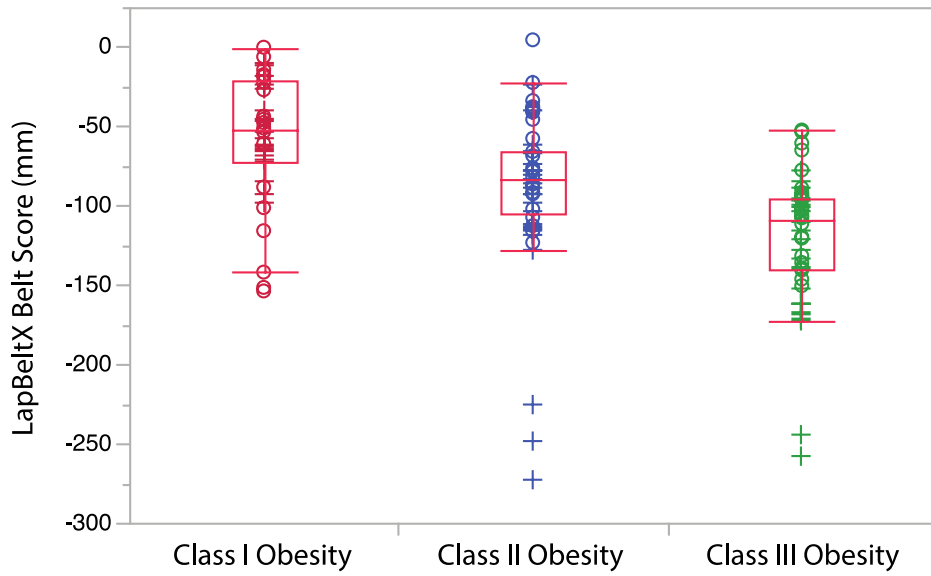


Figure 19. Box plot summaries the LapBeltX position by BMI classification. Box plots of the show median and interquartile range (IQR); whiskers indicate the maximum or minimum values within 1.5 IQR in distance from the nearest quartile of the LapBeltX.

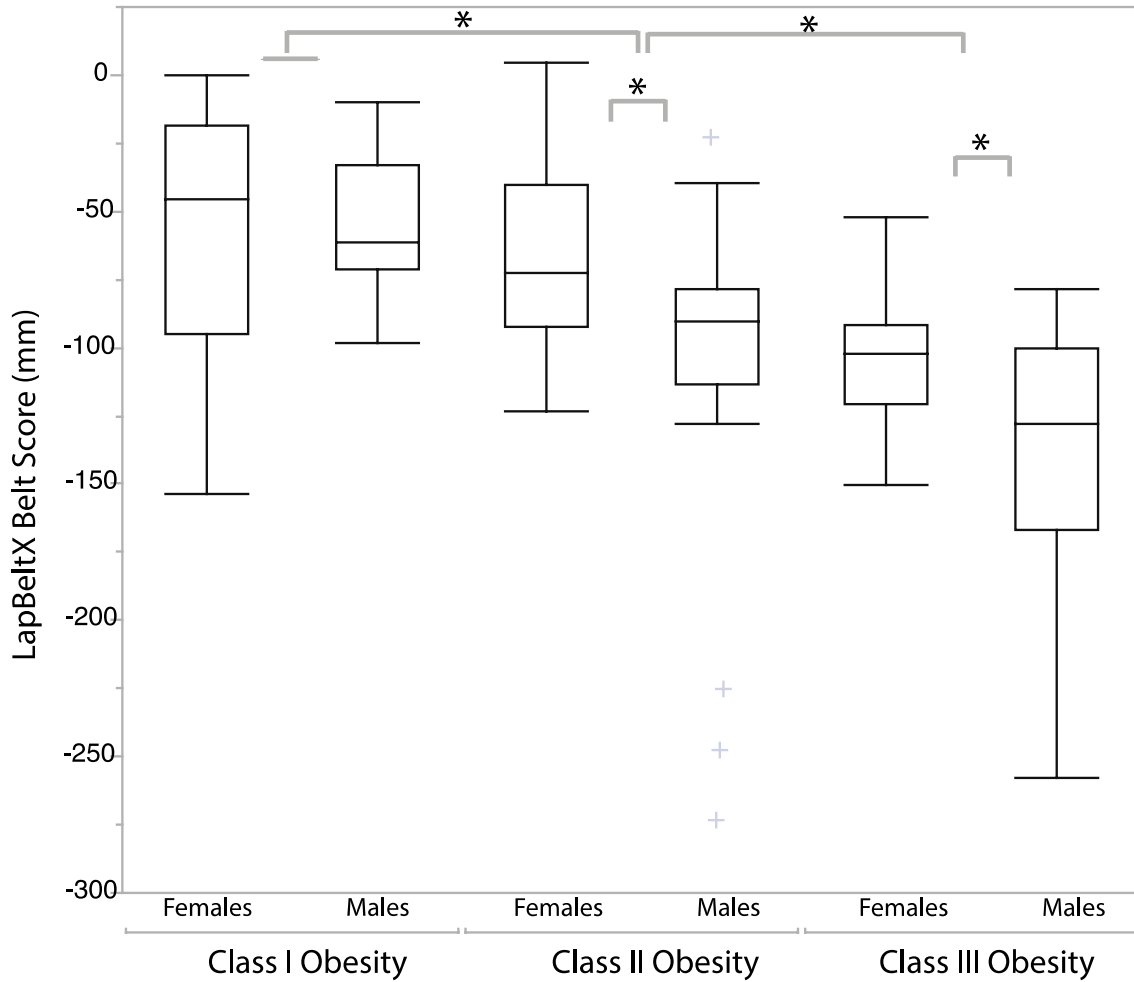


Figure 20. Box plot summaries the LapBeltX position by BMI classification and gender. Box plots of the show median and interquartile range (IQR); whiskers indicate the maximum or minimum values within 1.5 IQR in distance from the nearest quartile of the LapBeltX.

Age had a smaller effect than BMI, although inclusion of this effect and its interaction with gender did not improve the overall prediction of LapBeltX. Figure 21 illustrates the effect of BMI on LapBeltX, characterized by the age of the participants, younger (< 60 years) and older (60+ years) ($R^2=0.32$ and $R^2=0.45$).

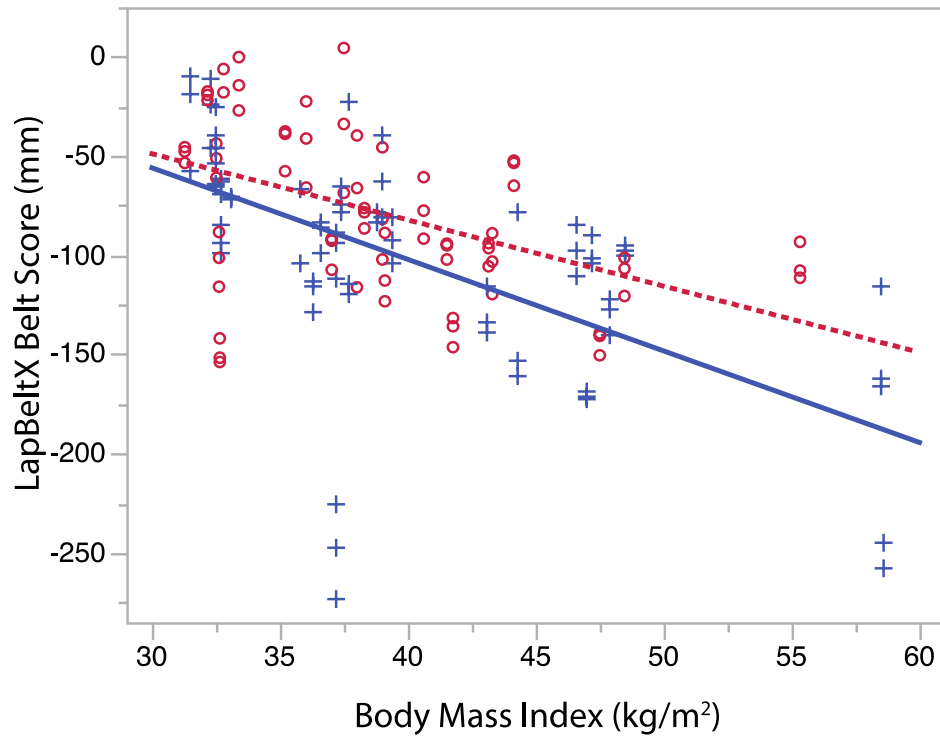


Figure 21. Effect of BMI on LapBeltX for women (o) and men (+) who are older (blue line, —) and younger (red line, - - -) than 60 years.

LapBeltZ

BMI was also the most important predictor of LapBeltZ, with higher BMI associated with belt positions farther forward and higher relative to the pelvis. The mean difference associated with a lap belt position was 25 mm relative to the pelvis across this cohort. Gender was also found to be a predictor of the Z location of the lap belt although to a lesser extent than BMI. Lap belt angle and stature were not found to be a significant predictor of LapBeltZ.

Table 10. Regression model predicting LapBeltZ (mm, $R^2_{adj} = 0.11$, RMSE=21.7).

Term	Estimate	Std Error	t Ratio	Prob> t
Intercept	26.64	11.07	2.41	0.0174*
BMI	0.9	0.27	3.26	0.0014*
Gender[F]	6.37	1.88	3.38	0.0009*

* For men, estimate is -6.37.

On average the female participants were found to position the lap belt 14 mm higher than males. The effect of BMI on LapBeltZ is shown for female ($R^2=0.14$) and male ($R^2=0.03$) participants in Figure 22.

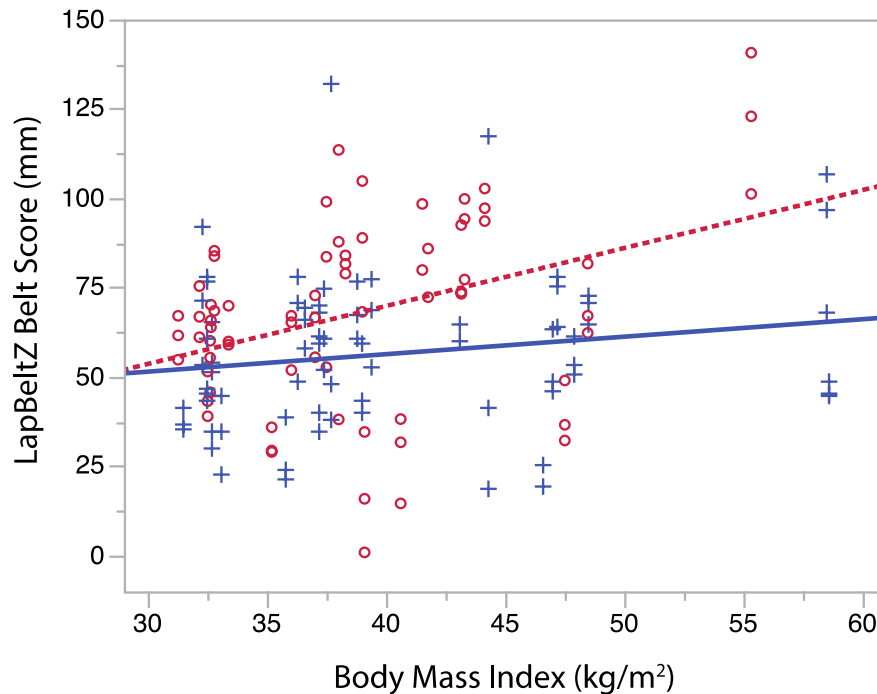


Figure 22. Effect of BMI on LapBeltZ for women (o, red line, - - -) and men (x, blue line, —).

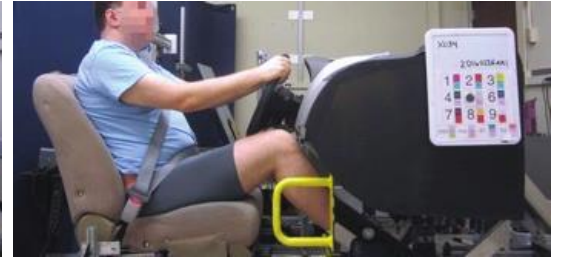


Figure 23. Example of belt fit for a participant (BMI=55.3 kg/m²; Stature=1633mm) for anchorage locations 30, 52, and 75 degrees to horizontal (left to right).

Female Participants

Male Participants

Class I Obesity
30-34.9 kg/m²



Class II Obesity
35-39.9 kg/m²



Class III Obesity
40-44.9 kg/m²



Class III Obesity
> 50 kg/m²



Figure 24. Photos showing lap belt fit for a range of occupant sizes (stratified by BMI classification).

Lap Belt Webbing Length

The length of belt webbing between the outboard anchorage and the latch plate was calculated from points digitized along the upper surface of the belt. Webbing length was strongly associated with seat position because the outer anchorage was attached to the mockup. Figure 25 shows the distribution of the lap belt length. The overall mean (SD) of the lap belt length was 1041 (117) mm.

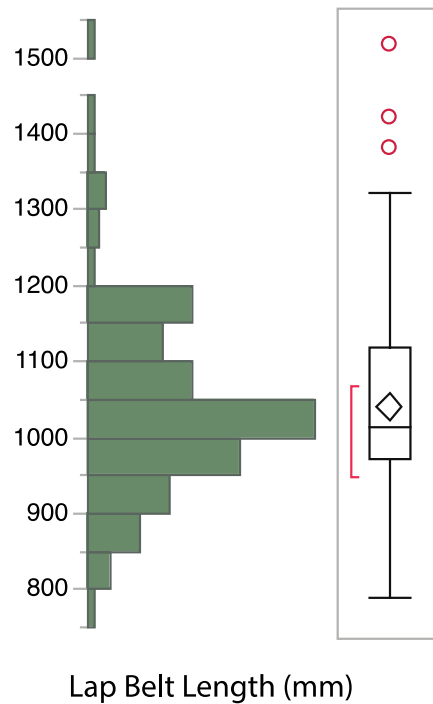


Figure 25. Distribution of the lap belt length (mm).

Regression analysis determined that BMI, seat position, and gender were significant predictors of lap belt length. Stature and age did not have a significant effect on lap belt length.

Table 11. Regression model predicting lap belt webbing length (mm, $R^2_{adj} = 0.48$, $RMSE=85.6$).

Term	Estimate	Std Error	t Ratio	Prob> t
Intercept	-399.28	358.98	-1.11	0.2680
Gender[F]*	28.47	7.2762	3.91	0.0001*
BMI	12.8	1.188	10.78	<.0001*
SeatHpoint_SubZ	1.68	0.62	2.73	0.0071*

* For men, estimate is -28.47.

The effect of BMI on lap belt length was approximately linear over the 728 mm range. The BMI slope of 12.8 mm (kg/m^2) and range of 27 kg/m^2 across the participants resulted in a difference of 350 mm of lap belt length. The highest BMI individuals had 350 mm lap belt webbing length more than the lowest BMI individuals in this sample, after accounting for vertical seat position. Median lap belt length values associated with Class I, II, and III obesity classifications are summarized in Figure 26. Significant differences were observed between lap belt lengths for participants classified by each level of BMI classification.

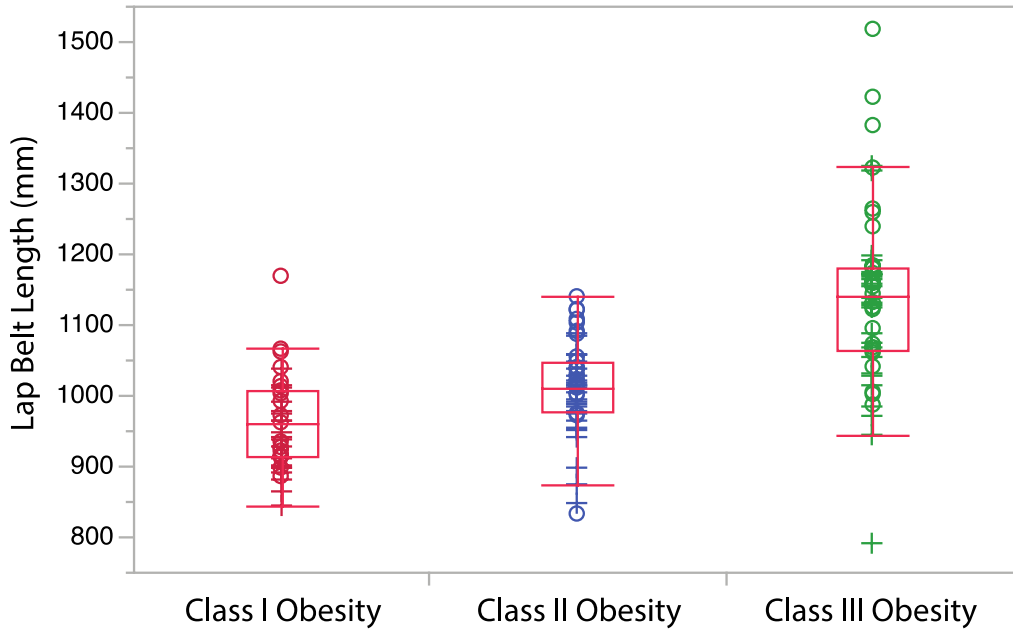


Figure 26. Box plot summaries the lap belt lengths (mm) by BMI classification. Box plots of the show median and interquartile range (IQR); whiskers indicate the maximum or minimum values within 1.5 IQR in distance from the nearest quartile of the lap belt length.

Lap belt length also differed by gender. After accounting for the vertical seat position, an average of 50 mm increase in lap belt length was observed for female participants. The effect of BMI on lap belt length is shown for female ($R^2 = 0.39$) and male ($R^2 = 0.53$) participants in Figure 27.

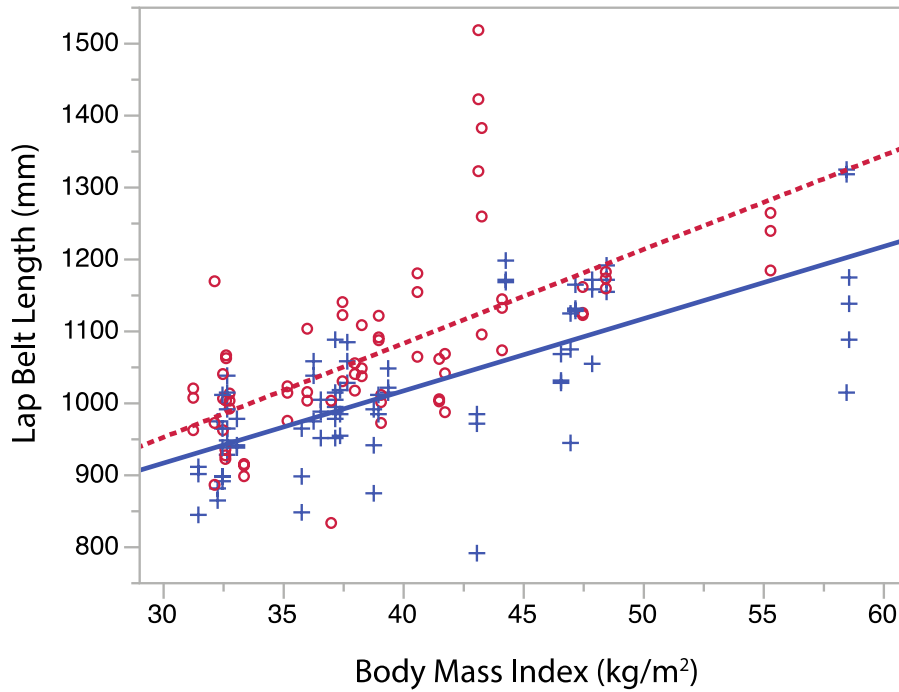


Figure 27. Effect of BMI on lap belt length for women (o, red line, - - -) and men (+, blue line, —).

Shoulder Belt Fit

Shoulder belt scores were analyzed for conditions DB1, DB4, and DB5. The shoulder belt score quantifies the location of the inner edge of the belt relative to the torso centerline at height of the suprasternale (Figure 16). A linear regression analysis was conducted to assess the effect of the YZ angle and participant covariates on the shoulder belt score and length of the torso belt.

Figure 28 shows the distribution of the shoulder belt score. The overall mean (SD) of the shoulder belt score for the high BMI cohort was -56 (38) mm.

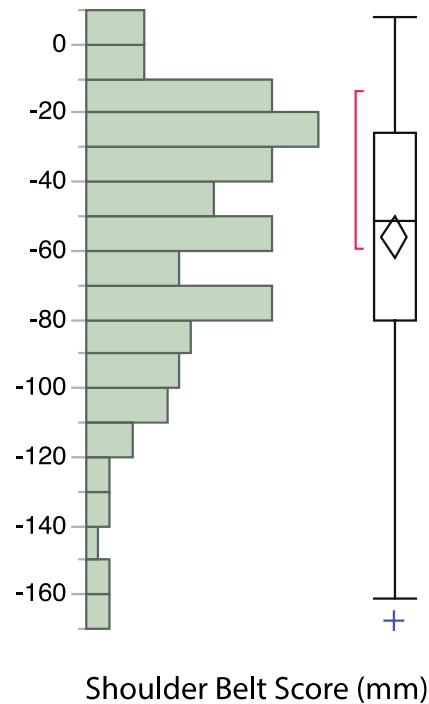


Figure 28. Distribution of the shoulder belt score (mm). Box plots of the show median and interquartile range (IQR); whiskers indicate the maximum or minimum values within 1.5 IQR in distance from the nearest quartile of shoulder belt score.

Shoulder Belt Score

Regression analysis determined that D-ring location (YZ angle), stature, and an interaction between YZ angle and gender effects were predictors of shoulder belt score. The YZ angle was the most important determinant of shoulder belt score. Table 12 shows a regression model that indicates that shoulder belt score was also affected by a two-way interaction. The adjusted R^2 for this model is 0.56.

Table 12. Regression model predicting shoulder belt score (mm, $R^2_{adj} = 0.53$, $RMSE=25.9$).

Term	Estimate	Std Error	t Ratio	Prob> t
Intercept	112.98	14.54	7.77	<.0001*
Gender[F]:(Stature -1698.58)	-0.07	0.039	-1.79	0.0759
Gender[M]:(Stature - 1698.58)	-0.15	0.039	-3.73	0.0003*
Gender[F]	-4.53	2.89	-1.57	0.1191
DringYZAngle	-7.96	0.68	-11.70	<.0001*
Gender[F]*(DringYZAngle -21.0832)	1.59	0.68	2.34	0.0206*

As anticipated, increased D-ring YZ angle was associated with larger (more outboard) shoulder belt scores. The range of D-ring anchorage locations resulted in a difference of 80 mm of the lateral displacement of the shoulder belt. Median shoulder belt scores values associated with YZ angle levels stratified by gender are summarized in Figure 29.

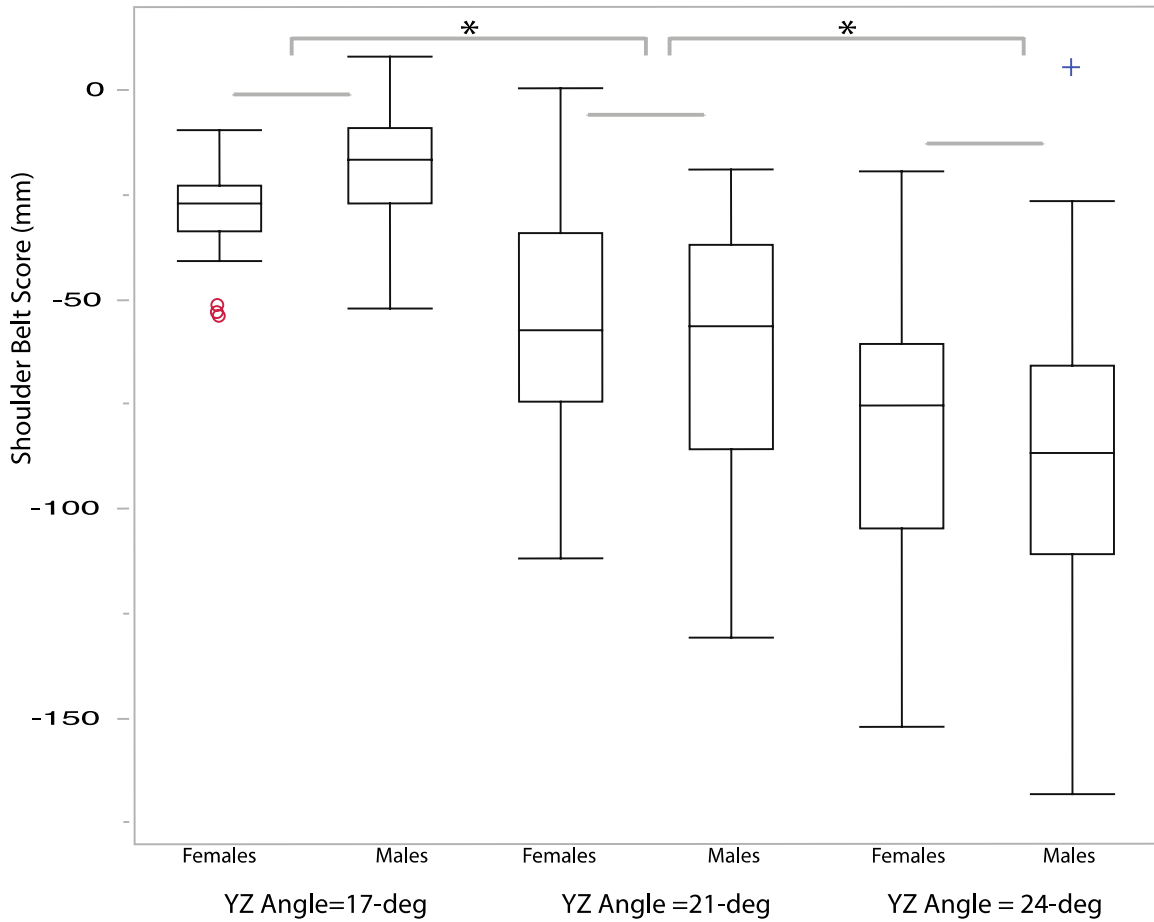


Figure 29. Box plot summaries of the shoulder belt scores by D-ring YZ angle level and gender (females- o, red & males-+,blue). Box plots of the show median and interquartile range (IQR); whiskers indicate the maximum or minimum values within 1.5 IQR in distance from the nearest quartile of shoulder belt score.

A significant interaction between gender and D-ring YZ angle was observed. During increased D-ring YZ angle conditions, the lateral displacement of the shoulder belt was on average 16 mm less for female participants. The effect of YZ angle on shoulder belt score is shown for female ($R^2 = 0.41$) and male ($R^2 = 0.54$) participants in Figure 30.

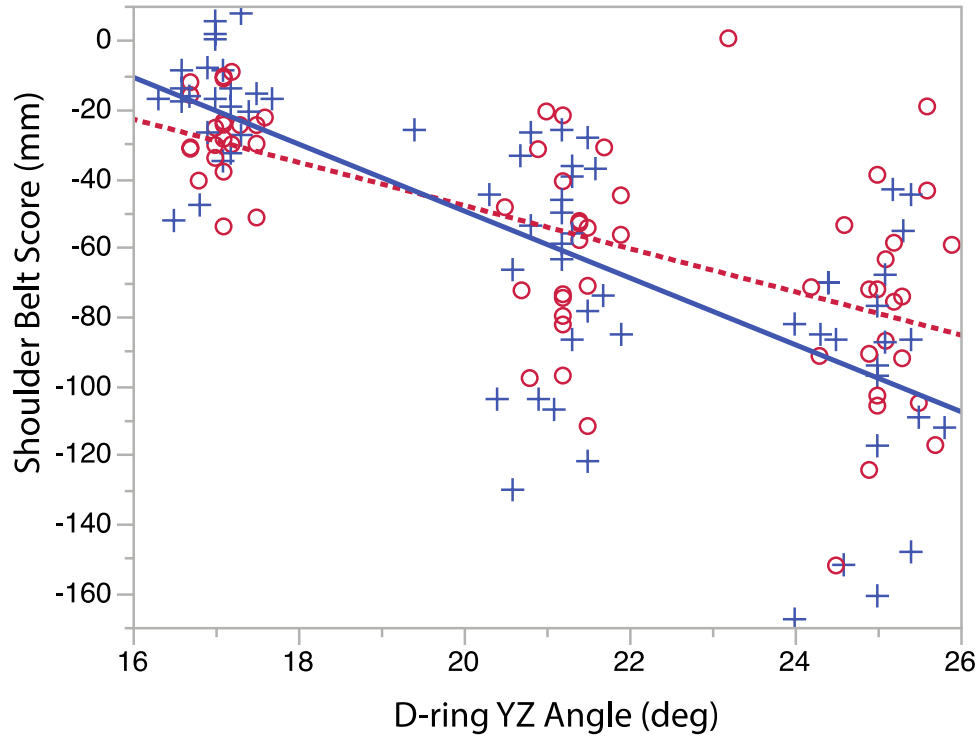


Figure 30. Effect of D-ring YZ on shoulder belt score for women (o, red line, -----) and men (+, blue line, ———).



Figure 31. Example of belt fit for participant (BMI=55.3 kg/m²; Stature=1633mm) for anchorage locations YZ angles of 17, 21, and 25 degrees (left to right).



Figure 32. Photos showing shoulder belt fit for a range of occupant sizes.

Torso Belt Length

The length of the torso belt between the D-ring (upper outboard anchorage) and the latchplate at the buckle was calculated from points digitized along the upper surface of the belt. Figure 33 shows the distribution of the shoulder belt length. The overall mean (SD) of the shoulder belt length was 888 (109) mm.

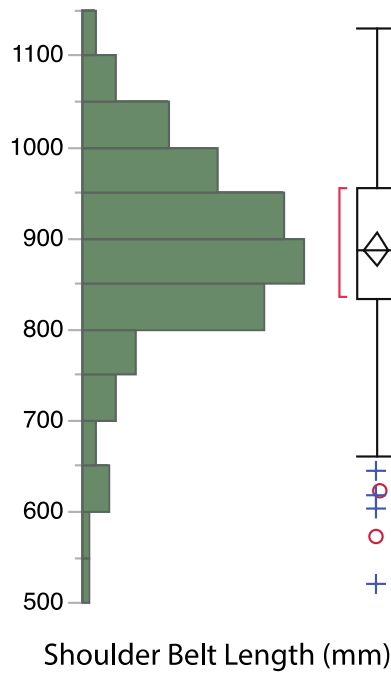


Figure 33. Distribution of the shoulder belt length (mm). Box plots of the show median and interquartile range (IQR); whiskers indicate the maximum or minimum values within 1.5 IQR in distance from the nearest quartile of the torso belt length.

Webbing length was strongly associated with the YZ belt angles, which moves the upper anchorage outward and rearward. After accounting for D-ring anchorage locations, regression analysis determined that stature, gender, and age were significant predictors of torso belt length.

Table 13. Regression model predicting shoulder belt length (mm, $R^2_{adj} = 0.50$, $RMSE=74.2$).

Term	Estimate	Std Error	t Ratio	Prob> t
Intercept	1251.04	46.99	26.63	<.0001*
Age at Testing	-1.21	0.44	-2.78	0.0062*
DringYZAngle	-14.80	1.94	-7.61	<.0001*
Gender[F]:(Stature -1699.83)	-0.67	0.11	-5.90	<.0001*
Gender[M]:(Stature - 1699.83)	-0.27	0.11	-2.34	0.0208*
Gender[F]	11.427	8.36	1.37	0.1742

The range of D-ring anchorage locations resulted in a difference of 148 mm of the shoulder belt webbing length. On average, a 92 mm additional belt webbing length between the D-ring and latch plate was observed for female participants.

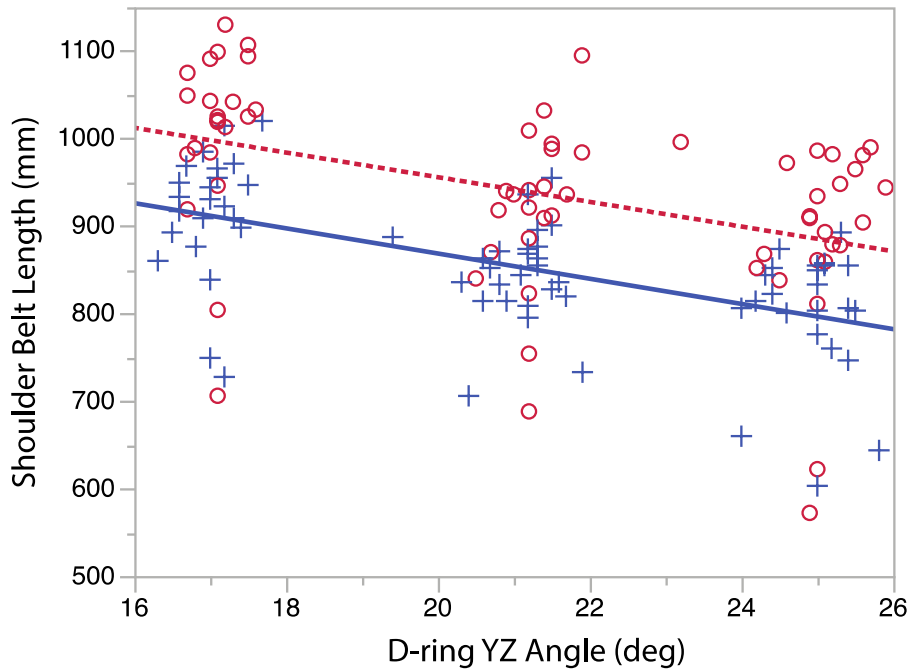


Figure 34. Effect of YZ angle on shoulder belt length for women (o, red, ----) and men (+, blue, —).

Age had a modest effect on shoulder belt length. Interactions were observed between gender, stature, and age although inclusion of these effects did not improve the overall prediction of shoulder belt length. Figure 35 illustrates the effect of stature on shoulder belt length, characterized by the age of the participants, younger (< 60 years) and older (60+ years) ($R^2=0.26$ and $R^2=0.36$).

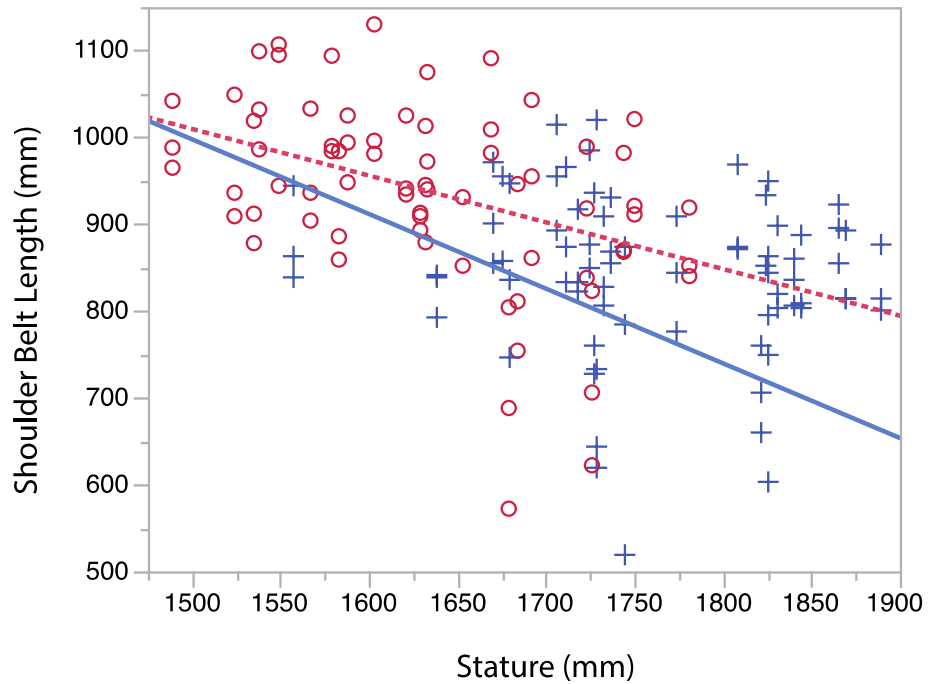


Figure 35. Effect of stature on shoulder belt length for women (o) and men (+) who are older (blue line, —) and younger (red line, - - -) than 60 years.

DISCUSSION

Lap belt fit was strongly affected by high levels of obesity. Higher BMI was associated with a lap belt position farther forward and higher relative to the pelvis, a finding that is consistent with previous research. Figure 36 shows a bivariate plot, demonstrating the distribution of the current obese cohort overlaid with the population from a previous study of driver belt fit (Reed et al., 2013).

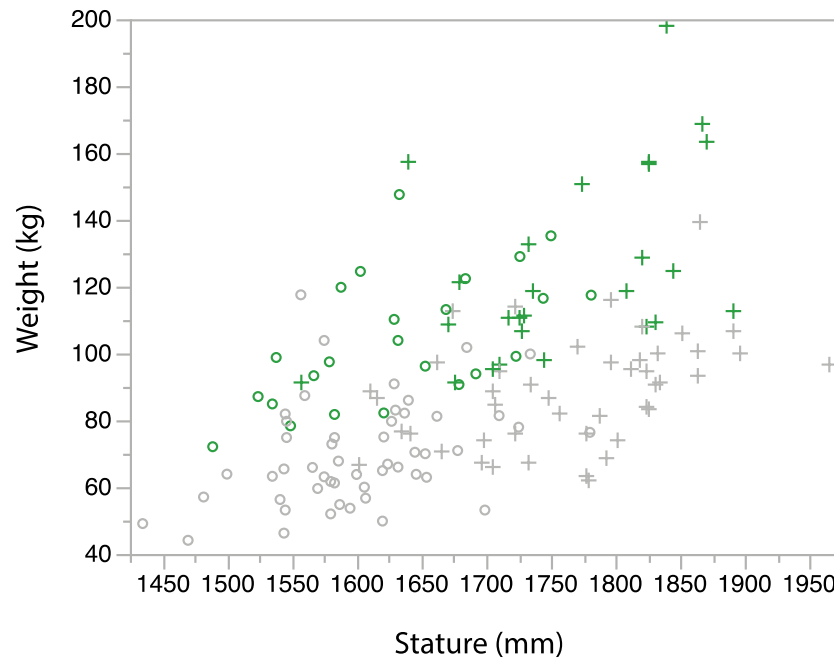


Figure 36. Distribution of the current obese participants (green) relative to the previous UMTRI belt fit study (grey) by Reed et al. (2013). Participants are coded by gender, women (o) and men (+).

The current study of obese drivers found that the fore-aft lap belt was located a mean of 32 mm farther forward of the anterior-superior iliac spine landmarks on the pelvis for each level of obesity classification. The effect of BMI on LapBeltX fit is similar across studies. For fore-aft lap belt, the coefficient of BMI was $-4.3 \text{ mm}/(\text{kg}/\text{m}^2)$ in Reed et al. (2012), $-5.1 \text{ mm}/(\text{kg}/\text{m}^2)$ in Reed et al. (2013), and $-4.3 \text{ mm}/(\text{kg}/\text{m}^2)$ in the current study. Figure 37 shows the lap belt location with respect to ASIS for men and women for all trials for the combined studies.

Increasing levels of obesity in the high level of obesity cohort had only a modest effect on the vertical placement of the lap belt. On average, higher BMI participants located the lap belt 62 mm above the ASIS. Reed et al. (2013) observed a mean of 34 mm and 58 mm higher relative to pelvis for participants classified as normal weight and overweight respectively. In the current study differences between participants of varying levels of obesity classification were not significant, suggesting a plateauing effect of the vertical lap belt location with respect to increasing BMI.

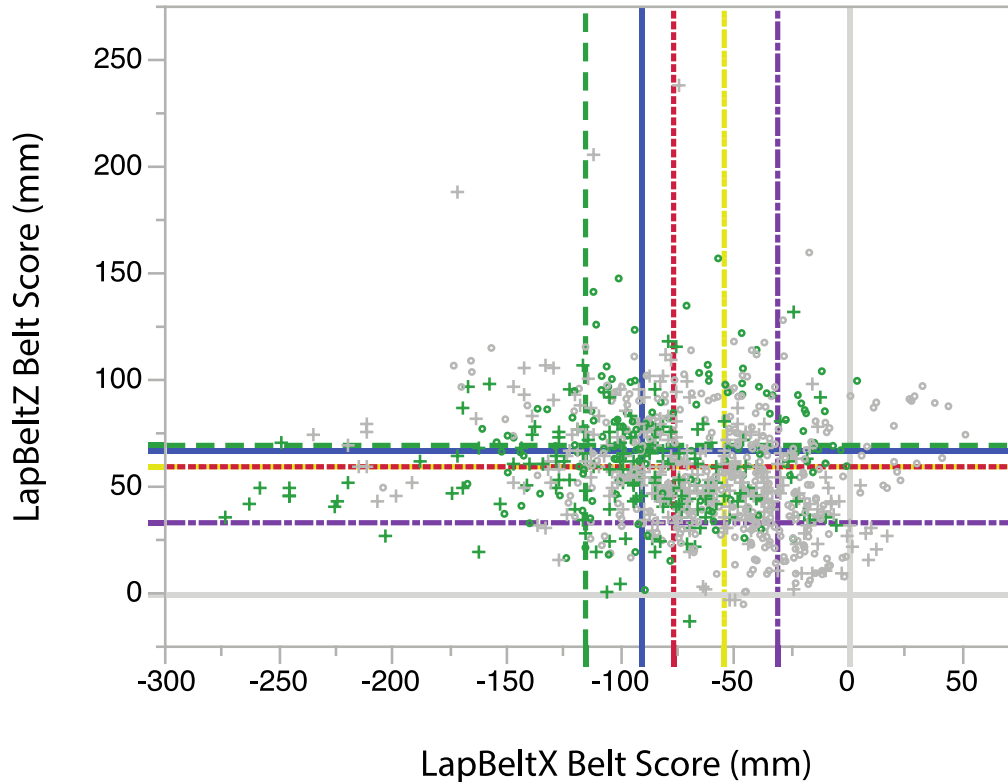


Figure 37. Lap belt location for all trials for women (o) and men (+) collapsed across the previous UMTRI driver (grey) and high BMI (green) study populations. Lines show the mean values of lap belt fit X and Z scores for each BMI classification: X=-31.2mm, Z=33.3mm for normal BMI (purple, ---), X=-54.7mm, Z=60.4mm for obese BMI (yellow, ---), X=-77.1mm, Z=60.1mm for Class I obesity, X=-91.8mm (red, ---), Z=66.9mm for Class II obesity (blue, ---), and X=-118.4mm, Z=68.2mm for Class III obesity (green, ---).

Higher BMI was also associated with greater length of lap belt webbing pulled from the retractor. For lap belt length, the coefficient of BMI was 12.9 mm/(kg/m²) in Reed et al. (2013) and 12.8 mm/(kg/m²) in the current study. Across the combined datasets, the range of BMI is 18.4 to 58.6 kg/m², which would result in a mean difference of 520 mm in lap belt length.

The effect of lap belt angle on the lap belt fit demonstrated in previous studies was not found with the current. Lap belt angle was associated with fore-aft belt position in both the Reed et al. (2013) and Reed et al. (2012) studies. It was also identified as a predictor of vertical lap belt position in the Reed et al. (2012) study. These results suggest that at higher BMI levels the body shape in the lower abdomen area dominates belt angle in determining fit.

Shoulder belt fit was less strongly affected by obesity than by the upper D-ring anchorage location. This finding is compatible with the previous studies. Reed et al. (2013) did not show any meaningful interactions between shoulder belt routing and participant characteristics after taking into account the geometric effects of

shoulder height (expressed as stature). However, for the current high-BMI cohort, the significant effect of gender nested within stature beyond the effects of overall body size. A significant interaction between the upper D-ring location and gender was also observed. Only at the smallest YZ angle did female participants show a larger shoulder belt score compared with male occupants. Differences in the female upper torso shape may cause the torso belt routing to deviate from bony landmarks at the sternum (Figure 32).

The effect of gender was unique to this study of belt fit for individuals with a high level of obesity. After accounting for stature and BMI, gender was associated with both lap and shoulder belt fit and length outcome measures. This finding is inconsistent with previous belt studies that excluded participants with BMI > 40 kg/m². Figure 24 illustrates representative belt fit stratified by BMI classification and gender. On average, female participants were observed to place the belt 12 mm above and 24 mm less forward of the anterior-superior iliac spine landmarks on the pelvis, as compared to male participants. Female participants also pulled out the lap belt 50 mm further relative to male participants. It is hypothesized that gender effects are a surrogate for body size and shape differences between women and men and that these differences are more pronounced in this higher BMI cohort. Further analysis of the 3D body shape data will be conducted to examine how body shape affects belt fit in this cohort.

Limitations

Testing was conducted in a laboratory vehicle mockup rather than in real vehicles. This static environment lacks some features of a vehicle and does not include potential effects of vehicle ride motion. The measurements were taken during short duration sitting sessions. Belt locations during longer duration driving could differ. The participants wore lightweight, standardized clothing and were observed as they donned the belt. Drivers in their own vehicles or wearing heavier clothing may don the belt differently.

Some methodological challenges arose due to the large variance in body shape in obese participants, in comparison with non-obese participants. Palpating bony landmarks needed for belt fit outcome measures is difficult, and landmark locations were often hard to determine as a result of skinfolds and soft-tissue deformation. Comorbidities related to mobility and joint range of motion are common in this cohort, challenging their ability to ingress and egress the driver mock-up and to maintain driving postures.

Conclusions and Implications

This study confirmed and extended previous findings regarding belt fit for individuals with high BMI. Increases in BMI are associated with approximately linear increases in the amount of fore-aft distance between the lap portion of the belt and the bony pelvis, as well as increases in the amount of belt webbing used. Both of these factors potentially diminish the effectiveness of the belt restraint. In a frontal crash, the ideal performance of the belt system includes rapid loading of the lap portion of the belt by the bony pelvis. The pretensioners in modern belt systems can remove some of the slack observed for individuals with high BMI, but the expected result of the observed lap belt positioning is high levels of forward translation before substantial lap belt force is generated.

This phenomenon of large lower-body excursions was demonstrated in a rear seating position by Forman et al. (2009a 2009b) in tests with obese post-mortem human subjects, who also showed that it could be mitigated to some extent by pretensioners. The situation for drivers is somewhat different, because an obese driver may interact with the knee bolster before substantial lap belt forces are developed, potentially leading to increased risk of lower-extremity injuries. More work is needed to determine the effects of obesity on restraint performance and to optimize restraint design for a wide range of BMI.

REFERENCES

- Carter, P.M., Flannagan, C.A.C., Reed, M.P., Cunningham, R.M., and Rupp, J.D. (2014). Comparing the effects of age, BMI and gender on severe injury (AIS 3+) in motor-vehicle crashes. *Accident Analysis and Prevention*. 72: 146–160.
- Centers for Disease Control and Prevention (CDC). <http://www.cdc.gov/>. Source adapted from: National Institutes of Health. Clinical guidelines on the identification, evaluation, and treatment of over- weight and obesity in adults: the evidence report. *Obesity Research*. 1998;6(suppl 2):51S-209S.
- Flegal, KM, Carroll MD, Ogden CL, Curtin LR. (2010). Prevalence and trends in obesity among US adults, 1999–2008. *JAMA*. 303:235–241.
- Forman, J., Lopez-Valdes, F., Lessley, D., Kindig, M., Kent, R., Ridella, S. and Bostrom, O., (2009a). Rear seat occupant safety: an investigation of a progressive force-limiting, pretensioning 3-point belt system using adult PMHS in frontal sled tests. *Stapp car crash journal* 53, 49.
- Forman, J., Lopez-Valdes, F.J., Lessley, D., Kindig, M., Kent, R. and Bostrom, O., (2009b). The effect of obesity on the restraint of automobile occupants. In *Annals of Advances in Automotive Medicine/Annual Scientific Conference*, p 25, Association for the Advancement of Automotive Medicine.
- Jehle D, Gemme S, Jehle C. (2012). Influence of obesity on mortality of drivers in severe motor vehicle crashes. *American Journal of Emergency Medicine*. 30:191-195.
- Kent RW, Forman JL, Bolstrom O. (2010). Is there really a “cushion effect”? a biomechanical investigation of crash injury mechanisms in the obese. *Obesity*. 18:749–753.
- Park, B-K and Reed, M.P. (2015). Parametric body shape model of standing children ages 3 to 11 years. *Ergonomics*. 10.1080/00140139.2015.1033480.
- Pasco, J.A., Brennan, S.L., and Kotowicz M.A. (2013). Morbid obesity in women on the rise: an observational, population-based study. *BMC Public Health*. 13:290. DOI:10.1186/1471-2458-13-290
- Reed, M.P., Ebert-Hamilton, S.M., and Hallman, J.J. (2013). Effects of Driver Characteristics on Seat Belt Fit. *Stapp Car Crash Journal*. 57:43-57.
- Reed, M.P., Ebert-Hamilton, S.M., and Rupp, J.D. (2012). Effects of obesity on seat belt fit. *Traffic Injury Prevention*, 13(4):364-372.
- Reed, M.P., Manary, M.A., and Schneider, L.W. (1999). Methods for measuring and representing automobile occupant posture. Technical Paper 990959. Proceedings of

the SAE International Congress and Exposition, Society of Automotive Engineers, Warrendale, PA.

Rupp, J.D., Flannagan, C.A.C, Leslie, A.J., Hoff, C.N., Reed. M.P., and Cunningham, R.M. (2013). Effects of BMI on the risk and frequency of serious injury in motor-vehicle crashes. *Obesity*. 21(1):88- 97

SAE International (2011). *SAE Handbook*. Warrendale, PA.

Sivak M, Schoettle B, Rupp J. (2010). Survival in fatal road crashes: body mass index, gender, and safety belt use. *Traffic Injury Prevention*. 11:66-68.

Sturm, R. (2007). Increases in morbid obesity in the USA: 2000–2005. *Public Health*. 121(7): 492–496.

Turkovich, M., van Roosmalen, L. (2010). A Preliminary study on the effects of obesity on occupant response in frontal impact. In: RESNA Annual Conference.

Turkovich M, Hu J, van Roosmalen L, and Brienza D (2013). Computer simulations of obesity effects on occupant injury in frontal impacts. *International Journal of Crashworthiness*. DOI:10.1080/13588265.2013.809646.

Viano DC, Parenteau CS, Edwards ML. (2008). Crash injury risks for obese occupants using a matched-pair analysis. *Traffic Injury Prevention*. 9:59–64.

Zhu S, Layde PM, Guse CE, et al. (2006). Obesity and risk for death due to motor vehicle crashes. *American Journal of Public Health*. 96:734–739.

APPENDIX A. Scripted Instructions

Introduction Script

Thank you for volunteering today. Over the next several hours, you will be participating in a scientific study investigating how people sit in vehicles. We are going to ask you to do some different things so that we can take measurements on your body.

First we will record the position of your body using a Faro Arm while you sit in different vehicle seats. An investigator will take the rounded tip of the arm and touch it to points on your body. A computer records the location of the tip. You will need to sit very still while we take these measurements.

We will also measure you by using a specialized set of rulers called anthropometers. We will measure the size of your head, arms, legs, hips, lower back, and chest.

Then we will record your body shape scanners. The scanners use different types of light to measure the outside surface of your body. The scanners do not produce X-rays, and are not like the scanners at the airport that can see through clothes. The scanner can only record the outside of your body and clothing. With the information from the scanners we can make a 3D computer models of the outside surface of your body. The full-body scanner uses red laser light, which is similar to the laser used at the checkout of a grocery store. The laser is safe for eyes. Each scan takes about 12 seconds, during which time you will have to stand or sit very still. We will also use 2 hand held scanners to record your shape for postures that are difficult to record with the full-body scanner. One is similar to the tracking technology of an X-Box Kinect gaming system and the other projects a light grid. These measurements will be made on you in three different positions: standing, sitting and laying down on your back.

We will also put marks on your skin with a pen, ink stamp, and body paint. They will be placed over skeletal landmarks and in a grid pattern on your torso. These marks help us take measurements on the computer. Please do not remove the marks until after we are finished, and let us know if one has fallen off or becomes smudged.

To perform these measurements, we will need you to wear special testing clothes. The scan clothing includes bicycle shorts and a swim cap. While sitting in the vehicle seats you will be wearing a cotton top over the scan clothes.

Driver Mockup Instruction Script

Overview: At this station we will ask you to sit in this driver seat, and then we will record your posture using this measurement arm.

I will feel for the location of a bone, then touch that location with this tip and press a button. The amount of rotation at each of these joints tells the computer where in space this tip is. It is similar to a mouse on a computer. I will record points on your head, neck, chest, hips, arms, and legs.

Please sit very still while we take the measurements otherwise we will have to start the measurements over. We will ask you to stand up at times so that we can make adjustments to the setup.

In the First Condition:

Please have a seat.

This is a simple seat but I am required to show you how the controls work. When you push this lever the seat back recline changes. Please try it out.

This button controls the up-down, forward-backward, and tilt of the seat cushion.
I will demonstrate. Please try it out.

Please place your right foot on the accelerator and your left foot flat on the floor. Then adjust the seat to a comfortable position for driving, as though you were going to be driving for a long time.

Please put on the seat belt.

Please sit as though you were driving with your hands on the steering wheel and your right foot on the accelerator and your left foot on the floor.

If they naturally sit centered left-right, in a symmetrical posture with the left foot flat on the floor and hands near the 2 and 10 position proceed to next instruction. Otherwise:

- If they are not centered left-right ask them to do so being sure to use the terms left and right, otherwise they might change their hip position forward-backward. For example say – Please move your rear-end left (or right) so that you are lined up with the seat.
- If their hands are in a different position or their feet are in some odd position, ask them to move their hands to 10 and 2, or place the left foot flat on the floor.
- If they say that this is how they usually or prefer to sit, say – I understand, but for this study we ask that everyone sit in a more standard driving position
- Further explanation if needed – We are not measuring your personal preference in this study, but rather how people's bodies fit in vehicles.

Relax your shoulders and look forward as though you are looking down the road.

This is the position that I will need you to “freeze” in while I take measurements. Please stay frozen until I tell you to “unfreeze.” I may move your hands so that I can reach points on your body, but please keep the rest of your body frozen.

After finishing measurements:

Now please be very careful as you step out to the right. Please stand or sit facing away from the seat while I set up the next condition.

Please return to the seat. I have moved the seat, so you'll need to adjust it again to get to your preferred position. Be sure to adjust the seat back angle, and adjust it forward and backward and up and down and the seat cushion tilt until you reach a comfortable posture.

Appendix B. Standard Anthropometry (measures unique to this study)

Definitions

Abdominal point, anterior - the most protruding point of the relaxed abdomen of a supine participant.

Buttock point, posterior – the point of maximum protrusion of the right buttock of a standing participant.

Chest point, right anterior - the most anterior point on the right side of the chest of a standing participant.

Omphalion- the center of the navel.

Abdominal Extension Depth, Supine

Description: The maximum depth of the abdomen when participant is supine.

Undrawn Landmark: Abdominal point, anterior.

Procedure: Participant is in a supine position with arms at their sides. Stand at the participant's right and use a stand caliper to measure the vertical distance between the anterior point of the abdomen and the top surface of the mattress. The abdomen is defined, in this case, as the area between the pectoral muscles and the crotch. The measurement is made at the maximum point of quiet respiration, without compression.

Instrument: Stand caliper.

CAUTION: Make sure the participant does not tense the abdominal muscles.

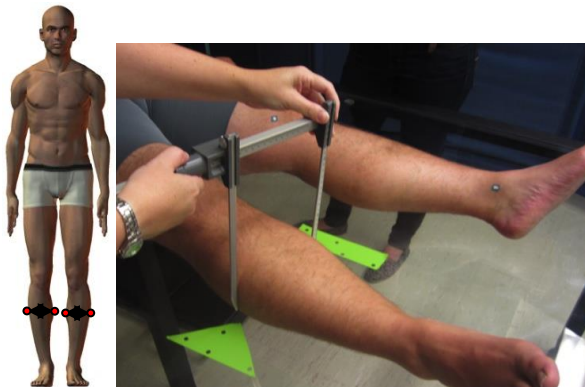


Calf Breadth, Left And Right, Supine

Description: The maximum breadth of the left and right calves when participant is supine.

Procedure: Participant is in a supine position with arms relaxed at the sides and feet pointing upwards. Stand at the right of the participant and use a small caliper to measure the maximum breadth of the right calf. Slide the caliper up and down the calf to ensure maximum breadth. Move to the left of the participant, and repeat on the left side. Exert only enough pressure to ensure that the caliper blades are making contact.

Instrument: Small caliper.



Circumference at Maximum Anterior Protrusion, Standing

Description: The maximum circumference of the chest at the fullest part of the breast.

Undrawn Landmark: Chest point, right anterior.

Procedure: Participant is in the anthropometric standing position. Stand in front of the participant and use a tape to measure the horizontal circumference of the chest at the level of the right chest point anterior landmark. This dimension will cross very soft tissue at the armpit and bust, and some compression of the tissue will inevitably occur. Be sure, however, to keep this to a minimum. The tape will span body hollows in this measurement. The measurement is taken at the maximum point of quiet respiration.

Instrument: Tape.



Circumference at Maximum Lateral Protrusion, Standing

Description: The horizontal circumference of the trunk at the level of the maximum lateral protrusion

Undrawn Landmark: Buttock point, posterior.

Procedure: Participant stands erect with the feet comfortably apart. Stand at the participant's right and use a tape to measure the horizontal circumference of the trunk at the level of the maximum lateral protrusion.

Instrument: Tape.

CAUTION: The tape must be maintained in a horizontal plane.



Circumference at Maximum Posterior Protrusion, Standing

Description: The horizontal circumference of the trunk at the level of the maximum protrusion of the right buttock.

Undrawn Landmark: Buttock point, posterior.

Procedure: Participant stands erect with the feet comfortably apart. Stand at the participant's right and use a tape to measure the horizontal circumference of the trunk at the level of the maximum protrusion of the right buttock. The tape should pass over the posterior buttock point (not drawn). Note if the pannus is included.

Instrument: Tape.

CAUTION: The tape must be maintained in a horizontal plane.



Front Chest Midline-Elbow Breadth, Supine

Description: The horizontal distance from the chest midline to the outside of the right elbow when participant is supine.

Procedure: Participant is in a supine position with arms relaxed at their sides. Stand at the right of the participant and use a large caliper to measure the horizontal distance from the midline of the chest to the outside of the right elbow.

Instrument: Large caliper.



Height of Maximum Anterior Protrusion, Standing

Description: The vertical distance between a standing surface and the height of maximum anterior protrusion.

Undrawn Landmark: Maximum anterior protrusion.

Procedure: Participant is in the anthropometric standing position with the feet comfortably apart. Stand in front of the participant and use a stand caliper to measure the vertical distance between the standing surface and the point of maximum anterior protrusion below the bust. The measurement is made at the maximum point of quiet respiration.

Instrument: Stand caliper.

CAUTION: The participant must not be allowed to tense the abdominal muscles.



Height of Omphalion, Standing

Description: The vertical distance between a standing surface and omphalion.

Undrawn Landmark: Waist (omphalion), anterior.

Procedure: Participant is in the anthropometric standing position with the feet comfortably apart. Stand in front of the participant and use a stand caliper to measure the vertical distance between the standing surface and the center of the navel (omphalion landmark). Ask the participant to identify the navel, and then place your finger at the indicated position. Ask the participant to look straight ahead, and then bring the caliper blade down to meet your finger. The measurement is made at the maximum point of quiet respiration.

Instrument: Stand caliper.

CAUTION: The participant must not be allowed to tense the abdominal muscles.



Height of Maximum Posterior Protrusion, Standing

Description: The vertical distance between a standing surface and the height of maximum posterior protrusion.

Undrawn Landmark: Maximum posterior protrusion.

Procedure: Participant is in the anthropometric standing position with the feet comfortably apart. Stand in front of the participant and use a stand caliper to measure the vertical distance between the standing surface and the point of maximum posterior protrusion. The measurement is made at the maximum point of quiet respiration.

Instrument: Stand caliper.

CAUTION: The participant must not be allowed to tense the abdominal muscles.



Navel Height, Omphalion, Standing

Description: The vertical distance between a standing surface and omphalion.

Undrawn Landmark: Waist (omphalion), anterior.

Procedure: Participant is in the anthropometric standing position with the feet comfortably apart. Stand in front of the participant and use a stand caliper to measure the vertical distance between the standing surface and the center of the navel (omphalion landmark). Ask the participant to identify the navel, and then place your finger at the indicated position. Ask the participant to look straight ahead, and then bring the caliper blade down to meet your finger. The measurement is made at the maximum point of quiet respiration.

Instrument: Stand caliper.

CAUTION: The participant must not be allowed to tense the abdominal muscles.



Stance Breadth, Standing

Description: The horizontal distance between the lateral surfaces of the ankles, while in a comfortable stance.

Undrawn Landmark: Lateral malleolus, left and right.

Procedure Participant stands with feet comfortably apart and with arms down at the sides. Stand in front of the participant and use a large caliper to measure the horizontal distance between the left and right lateral malleoli. Exert only enough pressure to ensure that the caliper blades are on the ankles.

Instrument: Large caliper.

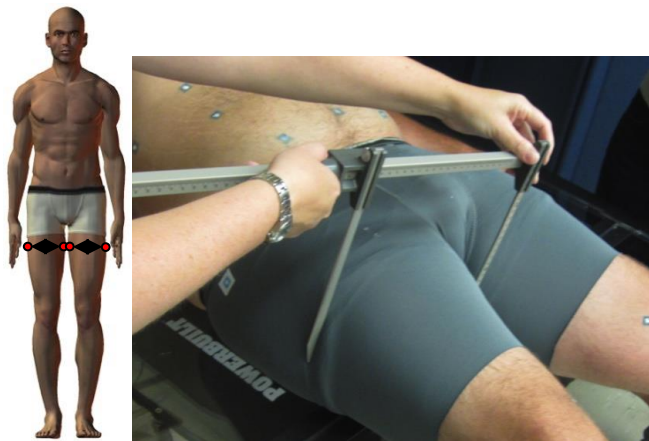


Thigh Breadth, Left And Right, Supine

Description: The maximum breadth of the left and right thighs when participant is supine.

Procedure: Participant is in a supine position with arms relaxed at their sides and feet pointing upwards. Ask participant to separate the legs if possible. Stand at the right of the participant and use a small caliper to measure the maximum breadth of the right thigh, perpendicular to the long axis of the thigh. Slide the caliper up and down the thigh to ensure maximum breadth. Move to the left of the participant, and repeat on the left side. Compress dress if worn.

Instrument: Small caliper.



Waist/Hip Breadth, Supine

Description: The maximum breadth of either the hips or the waist when the participant is supine.

Procedure: Participant is in a supine position with arms relaxed at their sides and feet pointing upwards. Stand at the right of the participant and use a large caliper to measure the maximum breadth of the hips or the waist. Slide the caliper up and down the lower torso to ensure maximum breadth. Note if the measurement is taken at the hips or the waist.

Instrument: Large caliper.



Waist Circumference, Supine

Description: The maximum horizontal circumference of the waist when participant is supine.

Procedure: Participant is in a supine position with arms relaxed at their sides and feet pointing upwards. Stand at the right of the participant and use a tape to measure the maximum horizontal circumference of the waist. Exert only enough tension on the tape to maintain contact between the tape and the body. The measurement is made at the maximum point of quiet respiration.

Instrument: Tape.



APPENDIX C. Whole-Body Scanning

Body shape and surface contours were recorded using a Vitronic Vitus XXL full-body laser scanner and Scanworx software by HumanSolutions. The VITUS XXL records hundreds of thousands of data points on the surface of the body in about 12 seconds by sweeping four lasers vertically. The two cameras on each of the four scanning heads pick up the laser light contour projected on the participant and translate the images into accurate three-dimensional data. Figure C1 shows participants in the scanner. In some postures, body regions of interest that were shadowed from the whole-body scanner were recorded using a handheld scanner. Handheld Artec 3D and Cubify Sense scanners were used to capture the supine scan posture on the transparent table.



Figure C1. Participants in full-body laser scanner

The scanner also records gray scale images that can be projected onto the 3D surface scan as shown in Figure C2. Body landmarks were marked on the skin using a pattern of water soluble, non-toxic, square ink stamp into which was placed a high contrast white paint dot. The complete list of skin markers are shown in Figures C4 and C5 and listed in Tables C1 and C4. Small hemispheres were taped to the shoulders of the soldiers to track the location of the acromion landmark.

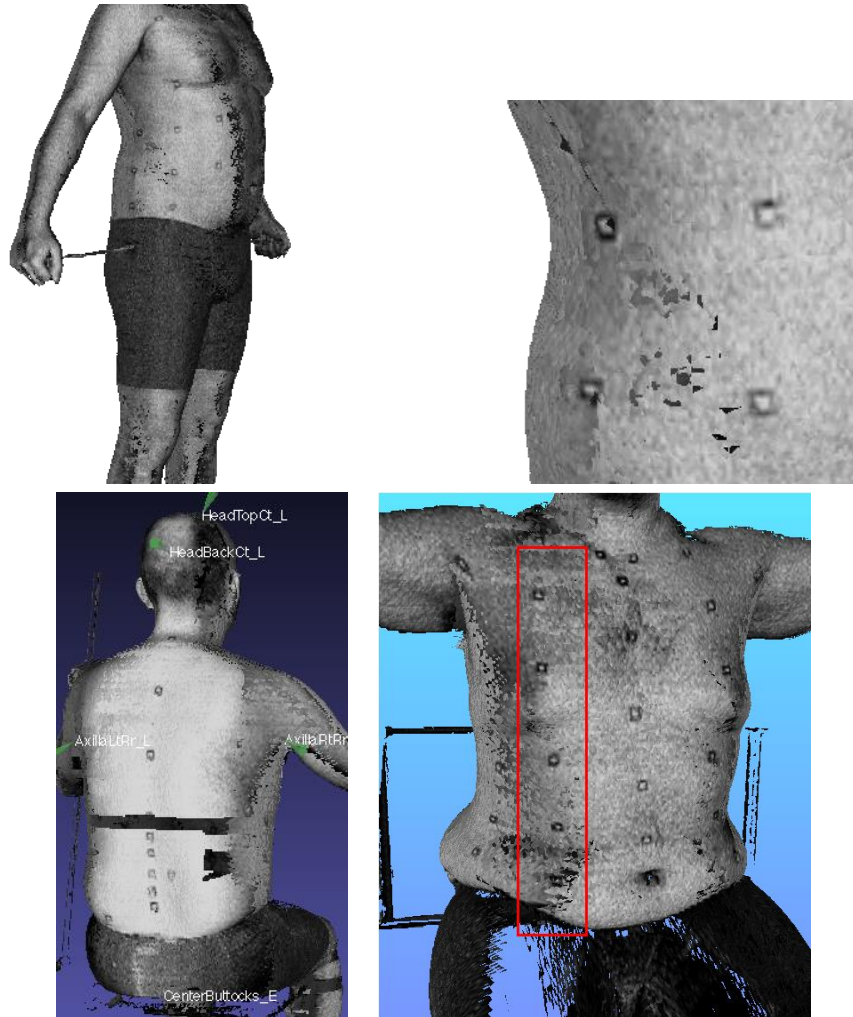


Figure C2. Examples of gray scale images projected onto a scan



Figure C3. Process of applying stamps to skeletal landmarks

Table C1. Scanning Marker List

Point Name	Body Part	Additional Description
AcromionLt_H	Torso	Center point on acromion hemisphere
AcromionRt_H	Torso	Center point on acromion hemisphere
ElbowMedLt_M	Arm	Medial epicondyle (mark with elbow bent 45°) (inside of elbow)
ElbowMedRt_M	Arm	Medial humeral epicondyle (mark with elbow bent 45°)
ElbowLatLt_M	Arm	Lateral epicondyle (mark with elbow bent 45°) (outside of elbow)
ElbowLatRt_M	Arm	Lateral humeral epicondyle (mark with elbow bent 45°)
WristMidTopLt_M	Arm	On the back of the wrist slightly proximal to the cross section plane of the ulnar styloid.
WristMidTopRt_M	Arm	On the back of the wrist slightly proximal to the cross section plane of the ulnar styloid.
WristMidBotLt_M	Arm	On the palm side of the wrist opposite the wrist mid marker
WristMidBotRt_M	Arm	On the palm side of the wrist opposite the wrist mid marker
KneeFemMedLt_M	Leg	Femoral epicondyle, medial
KneeFemMedRt_M	Leg	Femoral epicondyle, medial
KneeFemLatLt_M	Leg	Femoral epicondyle, lateral
KneeFemLatRt_M	Leg	Femoral epicondyle, lateral
AnkleLatLt_M	Leg	Malleolus, lateral
AnkleLatRt_M	Leg	Malleolus, lateral
AnkleMedLt_M	Leg	Malleolus, medial
AnkleMedRt_M	Leg	Malleolus, medial
SpineC07_M	Torso	Spinous process of the 7 th cervical vertebra (cervicale)
SpineT04_M	Torso	Spinous process of 4 th thoracic vertebra
SpineT08_M	Torso	Spinous process of 8 th thoracic vertebra
SpineT12_M	Torso	Spinous process of 12 th thoracic vertebra
SpineL01_M	Torso	Spinous process of 1st lumbar vertebra
SpineL02_M	Torso	Spinous process of 2nd lumbar vertebra
SpineL03_M	Torso	Spinous process of 3 rd lumbar vertebra
SpineL04_M	Torso	Spinous process of 4th lumbar vertebra
SpineL05_M	Torso	Spinous process of 5 th lumbar vertebra
SternSup22Y18Z_Lt_M	Torso	Marker 18 mm down and 22 to left of suprasternale
SternSub22Y18Z_Rt_M	Torso	Marker 18 mm down and 22 to right of suprasternale
SternSup60Z_Ct_M	Torso	Marker 60 mm down from suprasternale
TorsoMidUpperCt_M	Torso	Marker below the bottom of the sternum
TorsoMidLowerCt_M	Torso	Marker above the omphalion and below TorsoMidUpperCt_M
10RibLt_M	Torso	Marker on most lateral point on the 10 th rib
10RibRt_M	Torso	Marker on most lateral point on the 10 th rib
TorsoLt_M	Torso	Marker midway between 10Rib and Ilio
TorsoRt_M	Torso	Marker midway between 10Rib and Ilio
IlioLt_M	Torso	Marker on Iliocristale (most superior lateral point on pelvis)
IlioRt_M	Torso	Marker on Iliocristale (most superior lateral point on pelvis)

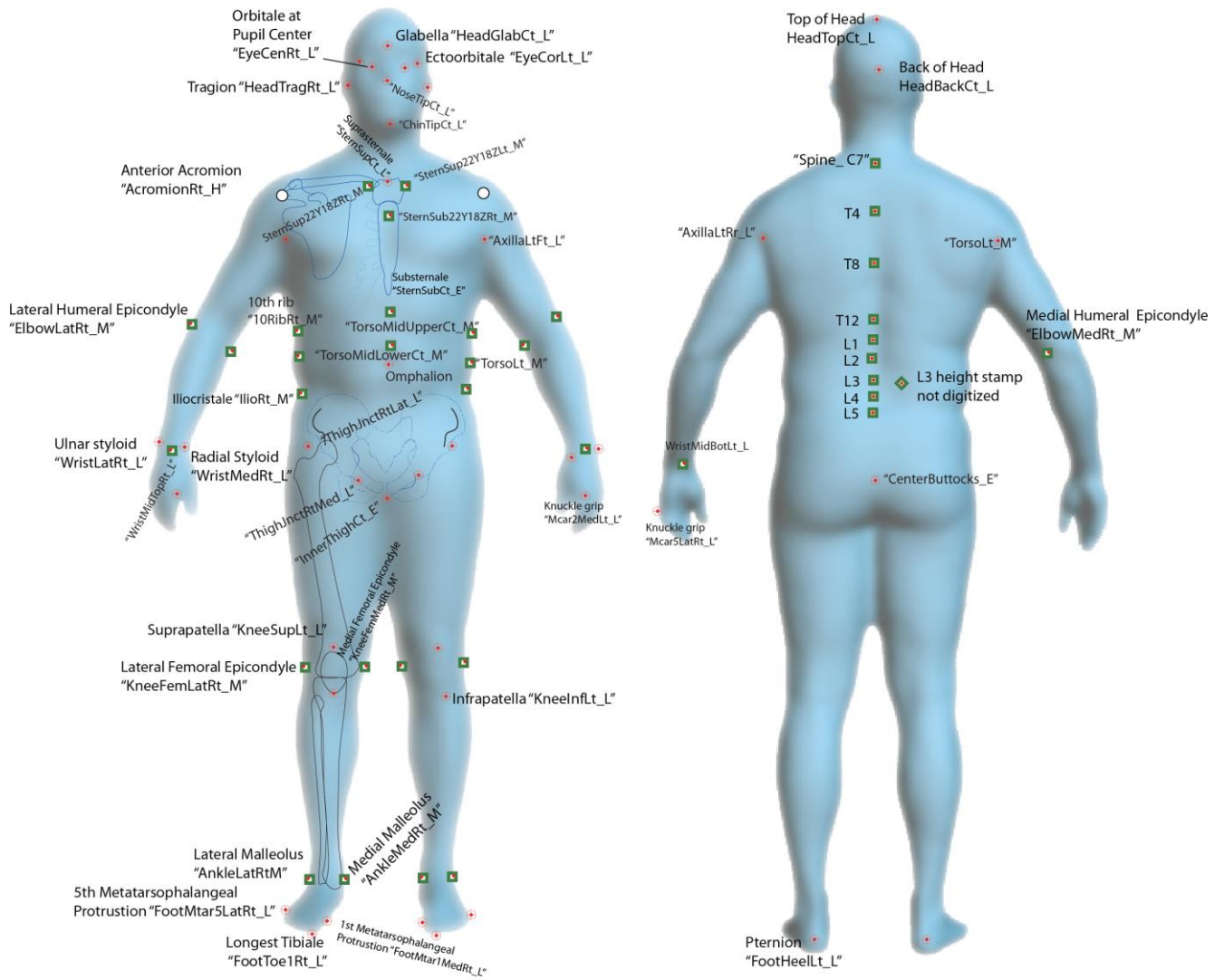


Figure C4. Markers stamped onto the skin (squares)

Table C2. Landmarks Digitized on Participant Scans with Gray Scale

Point Name	Body Part	Additional Description
HeadTopCt_L	Head	Most superior point on head or helmet
HeadBackCt_L	Head	Most posterior point on head or helmet
HeadTragLt_L	Head	Notch just above the tragus of the ear
EyeCorLt_L	Head	Point on orbit nearest the corner of eye
EyeCenLt_L	Head	Point on orbit below the eye at the same lateral position as the pupil when looking straight forward
HeadGlabCt_L	Head	Glabella: Smooth elevation of the frontal bone just above the bridge of the nose, between eyebrows
EyeCenRt_L	Head	Point on orbit below the eye at the same lateral position as the pupil when looking straight forward
EyeCorRt_L	Head	Point on orbit nearest the corner of eye
HeadTragRt_L	Head	Notch just above the tragus of the ear
NoseTipCt_L	Head	Tip of nose
ChinTipCt_L	Head	Menton (tip of chin)
WristLatLt_L	Arm	Styloid process on ulna (pinky side) – opposite of wrist “bump”
WristLatRt_L	Arm	Styloid process on ulna (pinky side) lateral point on wrist “bump”
WristMedLt_L	Arm	Styloid process on radius (thumb side) – opposite of wrist “bump”
WristMedRt_L	Arm	Styloid process on radius (thumb side) lateral point on wrist “bump”
Mcar5LatRt_L	Arm	Knuckle – grip axis, pinky side (5 th metacarpal medial)
Mcar2MedRt_L	Arm	Knuckle – grip axis, index side
Mcar2MedLt_L	Arm	Knuckle – grip axis, pinky side
Mcar5LatLt_L	Arm	Knuckle – grip axis, index side
SternSupCt_L	Torso	Anterior surface of jugular notch
SternSubCt_E	Torso	Substernale
InnerThighCt_E	Torso	Most inferior midline point on torso – mid crotch point
ThighJnctRtLat_L	Torso	Thigh – abdominal junction, lateral point (defining a line)
ThighJnctRtMed_L	Torso	Thigh – abdominal junction, medial point (defining a line)
ThighJnctLtMed_L	Torso	Thigh – abdominal junction, medial point (defining a line)
ThighJnctLtLat_L	Torso	Thigh – abdominal junction, lateral point (defining a line)
AxillaLtFt_L	Torso	Armpit Front (anatomical – not where the scan separates)
AxillaRtFt_L	Torso	Armpit Front
AxillaRtRr_L	Torso	Armpit Rear
AxillaLtRr_L	Torso	Armpit Rear
CenterButtocks_E	Torso	Most posterior midline point on the buttocks
FootMtar5LatLt_L	Leg	Ball of foot lateral (metatarsal-phalangeal protrusion)
FootMtar5LatRt_L	Leg	Ball of foot lateral
FootMtar1MedLt_L	Leg	Ball of foot medial
FootMtar1MedRt_L	Leg	Ball of foot medial
FootToe1Lt_L	Leg	Acropodian (most distal phalangeal point)
FootToe1Rt_L	Leg	Acropodian (most distal phalangeal point)
FootHeelRt_L	Leg	Most posterior point on right heel
FootHeelLt_L	Leg	Most posterior point on left heel
KneeSupLt_L	Leg	Most proximal point on left patella
KneeInfLt_L	Leg	Most distal point on left patella
KneeSupRt_L	Leg	Most proximal point on right patella
KneeInfRt_L	Leg	Most distal point on right patella

Table C3. Landmarks Digitized on Participant Scans with Avatar Surface

Point	Description
Gonion_Rt_L	jaw corner
Gonion_Lt_L	
BustPoint_Rt_L	most anterior point on pectoral muscle or bust (areola)
BustPoint_Lt_L	
Infrathyroid_Ct_L	Adams apple
Omphalion_Ct_L	Belly button (or center of belly button crease)
ArmUpperAntLt_E	<p>3 points on each limb segment. These points ring-around the middle of each segment on the anterior, posterior and lateral surfaces as determined in a neutral standing position. Nothing on the medial surface, as the inner thighs and inner arms usually do not scan well. Note: the anterior arm point will be pointing posterior when the shoulder is flexed (A1)- but still digitize the point on the biceps...etc</p> <p>The ring (anterior-lateral-posterior) of points form a plane PERPENDICULAR to the LONGITUDINAL AXIS of the limb.</p>
ArmUpperLatLt_E	
ArmUpperPosLt_E	
ArmLowerAntLt_E	
ArmLowerLatLt_E	
ArmLowerPosLt_E	
ArmUpperAntRt_E	
ArmUpperLatRt_E	
ArmUpperPosRt_E	
ArmLowerAntRt_E	
ArmLowerLatRt_E	
ArmLowerPosRt_E	
LegUpperAntLt_E	
LegUpperLatLt_E	
LegUpperPosLt_E	
LegLowerAntLt_E	
LegLowerLatLt_E	
LegLowerPosLt_E	
LegUpperAntRt_E	
LegUpperLatRt_E	
LegUpperPosRt_E	
LegLowerAntRt_E	
LegLowerLatRt_E	
LegLowerPosRt_E	
ThighJnctMidlineRt_L	On the top (anterior) midline of the thigh where it contacts the abdomen - must be done on avatar
ThighJnctMidlineLt_L	
CrotchMidThighHtCt_L	Center of crotch at the mid-thigh height - must be done on the avatar

Torso Grid Landmarks

A grid pattern of landmarks was also stamped on the participant's torso during a standing posture (Figures C5-C16). The centerline (S0-S4) was established at equally spaced distances between the sternum marker and a marker placed just below the omphalion. Two vertically oriented lines (A0-A4), located directly bilateral to the centerline (anterior), were defined by equally spaced distances between a marker at the sternum height, placed halfway between the centerline (anterior) and axilla, and a marker placed at the height just below the omphalion. Markers were located along the sagittal plane at the height of the 10th rib, iliocristale, and at the mid-point. Markers along the spine (posterior) were defined at T12, L3 and L5. The remaining markers were set at halfway points on the horizontally oriented lines connecting the bilateral to centerline (A0-A4) and spine (posterior) markers with the sagittal markers. If additional markers were required to capture the panniculus below the omphalion in the supine posture, the vertically oriented grid pattern was extended at same spacing as used when standing. The objective of the torso grid pattern was to track surface shape and deformation differences between scan postures.

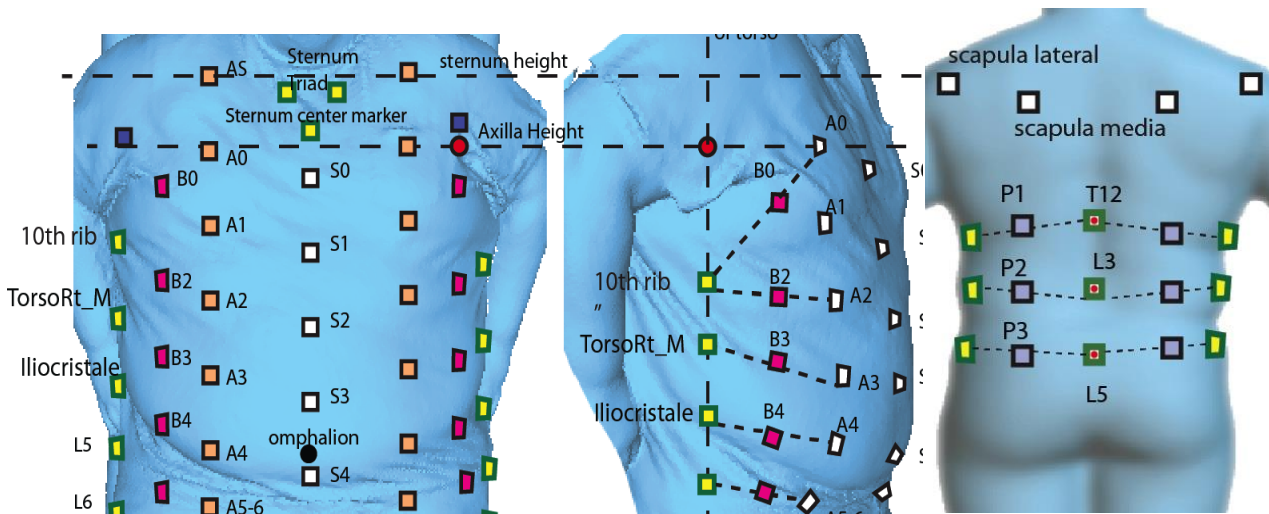


Figure C5. Illustration of markers stamped onto the participants' torsos



Figure C6. Torso grid markers stamped on participants' skin and taped to sports bra

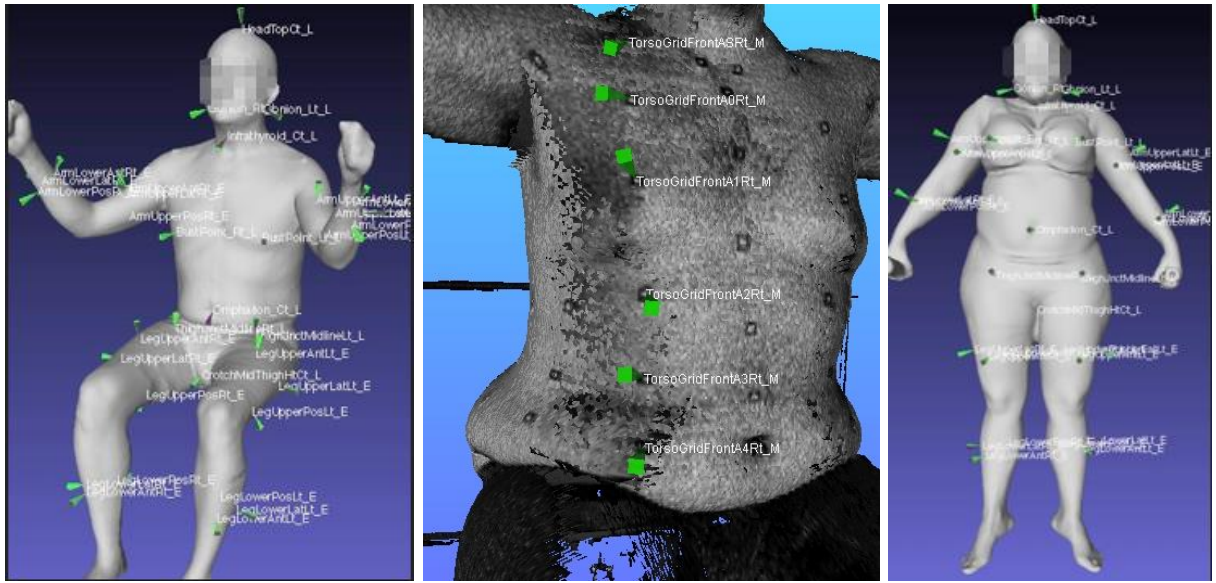


Figure C7. Examples of makers and landmarks digitized on scans



Figure C8. Marking 10RibLt_M and IlioLt_M

Table C4. Scanning Marker List for Torso Grid

Point Name	Body Region	Additional Description
TG_Frt_AxillaRt_M	Torso	Marker above right front armpit
TG_Frt_AxillaLt_M	Torso	Marker above left front armpit
TG_Frt_CtS0_M	Torso	1 st Marker down the center of the front of the torso
TG_Frt_CtS1_M	Torso	2 nd Marker down the center of the front of the torso
TG_Frt_CtS2_M	Torso	3 rd Marker down the center of the front of the torso
TG_Frt_CtS3_M	Torso	4 th Marker down the center of the front of the torso
TG_Frt_CtS4_M	Torso	5 th Marker down the center of the front of the torso, just below belly button
TG_Frt_ExtraCtS5_M	Torso	6 th Marker down the center of the front of the torso – optional
TG_Frt_ExtraCtS6_M	Torso	7 th Marker down the center of the front of the torso – optional
TG_Frt_ASlt_M	Torso	1 st Marker at suprasternale height to the right of the centerline
TG_Frt_A0Lt_M	Torso	2 nd Marker in the line to the left of the centerline
TG_Frt_A1Lt_M	Torso	3 rd Marker in the line to the left of the centerline
TG_Frt_A2Lt_M	Torso	4 th Marker in the line to the left of the centerline
TG_Frt_A3Lt_M	Torso	5 th Marker in the line to the left of the centerline
TG_Frt_A4Lt_M	Torso	6 th Marker in the line to the left of the centerline
TG_Frt_ExtraA5Lt_M	Torso	7 th Marker in the line to the left of the centerline – optional
TG_Frt_ExtraA6Lt_M	Torso	8 th Marker in the line to the left of the centerline – optional
TG_Frt_B0Rt_M	Torso	Marker between 10RibRt_M and A0Rt_M
TG_Frt_B2Rt_M	Torso	Marker between 10RibRt_M and A2Rt_M
TG_Frt_B3Rt_M	Torso	Marker between TorsoRt_M and A3Rt_M
TG_Frt_B4Rt_M	Torso	Marker between IlioRt_M and A4Rt_M
TG_Frt_ExtraB5Rt_M	Torso	Marker between ExtraL5Rt_M and ExtraA5Rt_M
TG_Frt_ExtraB6Rt_M	Torso	Marker between ExtraL6Rt_M and ExtraA6Rt_M
TG_Frt_B0Lt_M	Torso	Marker between 10RibLt_M and A0Lt_M
TG_Frt_B2Lt_M	Torso	Marker between 10RibLt_M and A2Lt_M
TG_Frt_B3Lt_M	Torso	Marker between TorsoLt_M and A3Lt_M
TG_Frt_B4Lt_M	Torso	Marker between IlioLt_M and A4Lt_M
TG_Frt_ExtraB5Lt_M	Torso	Marker between ExtraL5Lt_M and ExtraA5Lt_M
TG_Frt_ExtraB6Lt_M	Torso	Marker between ExtraL6Lt_M and ExtraA6Lt_M
TG_Sde_Extra5Lt_M	Torso	1 st Marker below IlioLt in line with A5Lt_M
TG_Sde_Extra5Lt_M	Torso	2 nd Marker below IlioLt in line with A6Lt_M
TG_Sde_Extra5Rt_M	Torso	1 st Marker below IlioRt in line with A5Rt_M
TG_Sde_Extra5Rt_M	Torso	2 nd Marker below IlioRt in line with A6Rt_M
TG_Bck_ScapulaMedLt_M	Torso	Marker on left scapula, medial
TG_Bck_ScapulaMedRt_M	Torso	Marker on right scapula, medial
TG_Bck_ScapulaLatLt_M	Torso	Marker on left scapula, lateral
TG_Bck_ScapulaLatRt_M	Torso	Marker on right scapula, lateral
TG_Bck_P1Lt_M	Torso	Marker on back between T12_M and 10thRibLt
TG_Bck_P2Lt_M	Torso	Marker on back between L3 and TorsoLt_M
TG_Bck_P3Lt_M	Torso	Marker on back between L5 and IlioLt_M
TG_Bck_P1Rt_M	Torso	Marker on back between T12_M and 10thRibRt
TG_Bck_P2Rt_M	Torso	Marker on back between L3 and TorsoRt_M
TG_Bck_P3Rt_M	Torso	Marker on back between L5 and IlioRt_M



Figure C9. Marking TorsoLt_M and extending side marks down to TG_Sde_Extra5Rt_M



Figure C10. Marking TG_Bck_P1Lt_M through TG_Bck_P4Lt_M



Figure C11. TG_Frt_CtS0_M through TG_Frt_CtS4_M and extra TG_Frt_ExtraCtS5_M



Figure C12. Marking TG_Frt_AxillaLt_M



Figure C13. Finding TG_Frt_A1Lt_M



Figure C14. Marking TG_Frt_ASlt_M through TG_Frt_A4Lt_M and extras TG_Frt_ExtraA5Lt_M

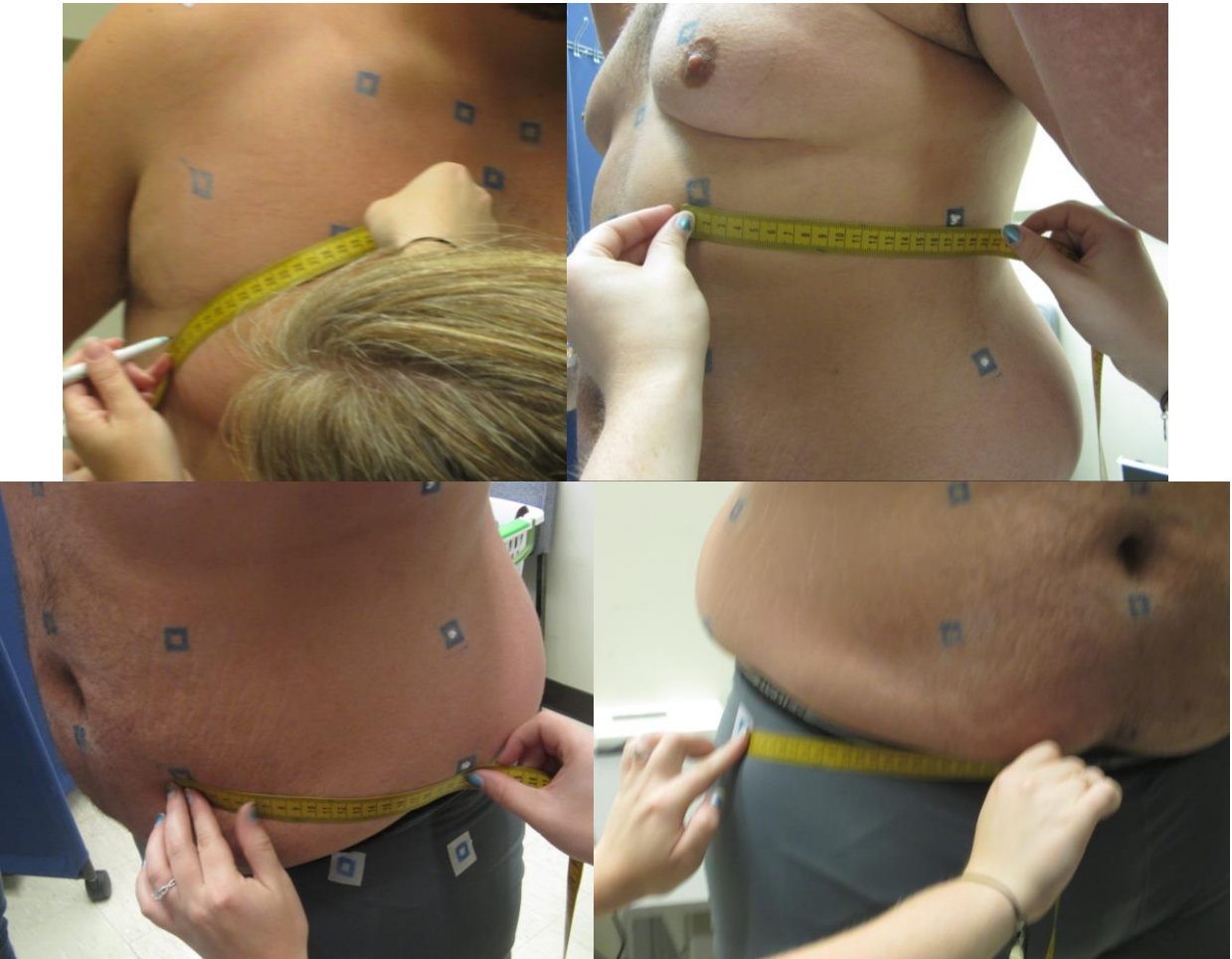


Figure C15. Marking TG_Frt_B0Lt_M through TG_Frt_B0Lt_M and extras TG_Frt_ExtraB5Lt_M



Figure C16. Completed torso grid marking

Scan Postures

Participants were scanned in 27 postures listed in Table C5. Postures included standing, sitting, and supine. The “recline” scans were a series of three postures in which the participant’s posture went from erect to very reclined, while maintaining a 90° knee angle with legs and feet parallel. To achieve scan coverage of the sides of the torso, the participants’ arms were moved away from the body, but the shoulder position was kept in a relaxed seat position. The investigator set the elbow angle to 120°, the angle of the arm relative to the midline of the torso in coronal view to 45°, and the hand height to the suprasternale height in the erect posture. Participants were instructed to sit looking forward with relaxed shoulders with the weight of the arms and support by gripping an upright rod and with a relaxed spine in the two more recline postures.

Table C5. Automotive, Standing and Standard Scanning Postures

Posture	#	Seat Pan	Seat Back	Hips	Lower Limbs	Spine	Shoulders	Hand Scan
Standing Feet Natural	T0	N/A	N/A	N/A	Natural	Natural	Natural	
Standing Natural	T1	N/A	N/A	N/A	15 cm	Natural	Natural	
Standing Abduction	T2	N/A	N/A	N/A		Natural	Abduction 40°	
Standing Erect	T3	N/A	N/A	N/A		Erect	Abduction 40°	
Standing T-pose	T4	N/A	N/A	N/A	45 cm	Natural	Abduction 90°	
Car – body	CB	14.5°	Support	Natural	Driving Thighs Parallel	Natural	Handles	Yes
Car – feet	CF							Yes
Recline 1 (min)	R1	14.5°	Support	Natural	Knees 90° Thighs Parallel	Min recline	Handles	Yes
Recline 2 (mid)	R2					Mid recline		Yes
Recline 3 (max)	R3					Max recline		Yes
Sling 0°, knee 90°	S3	0°	Support	Natural	Knees 90° Natural Splay	0° recline	Handles	Yes
Sling 20°, knee 90°	S4					20° recline		Yes
Sling 0, knee 60°	S1				Knees 60° Natural Splay	0° recline		Yes
Sling 20°, knee 60°	S2					20° recline		Yes
Sitting Lap	L1	0°	No Support	75°	Legs and feet symmetrical with thighs parallel, ankles under the knees, and feet parallel	Erect	Handles	
Spine Flexion Min/Nat	V1	0°	No Support	75°	Ankle under knees (L1) Thighs parallel	Relaxed	Handles	
Spine Flexion Max	V2					Maximum Flexion		
Spine Flexion Mid	V3					Flexion between V1 and V2		
Spine Rotation Right	V5					Maximum Rotation to Right		
Spine Rotation Left	V6					Maximum Rotation to Left		
Hip Flexion Max	V7					Maximum Flexion		
Hip Flexion Comfort	V8	Comfortable Flexion	Flexion					
Shoulder Flex 90°	A1	0°	No Support	75°	Ankle under knees (L1)	Erect	90° Flexion	
Shoulder Flex Max	A2						Maximum Flexion	
Shoulder Abd. 90°	A3						90° Abduction	
Shoulder Abd. Max	A4						Maximum Abduction	
Shoulder Ext Max	A5						Maximum Extension	
Arms “Y”	AY						Arms in “Y” position	

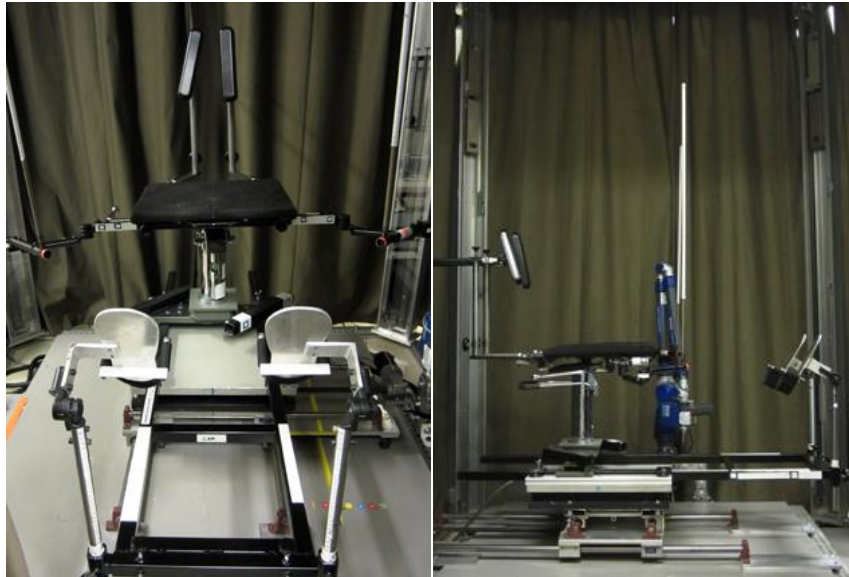


Figure C17. Scanner set up for driver automotive posture, H30=270 mm, back angle = 23°



Figure C18. Participant in full-body scanner seat in automotive posture with investigator also using a hand-held scanner to record the shape of the lap area

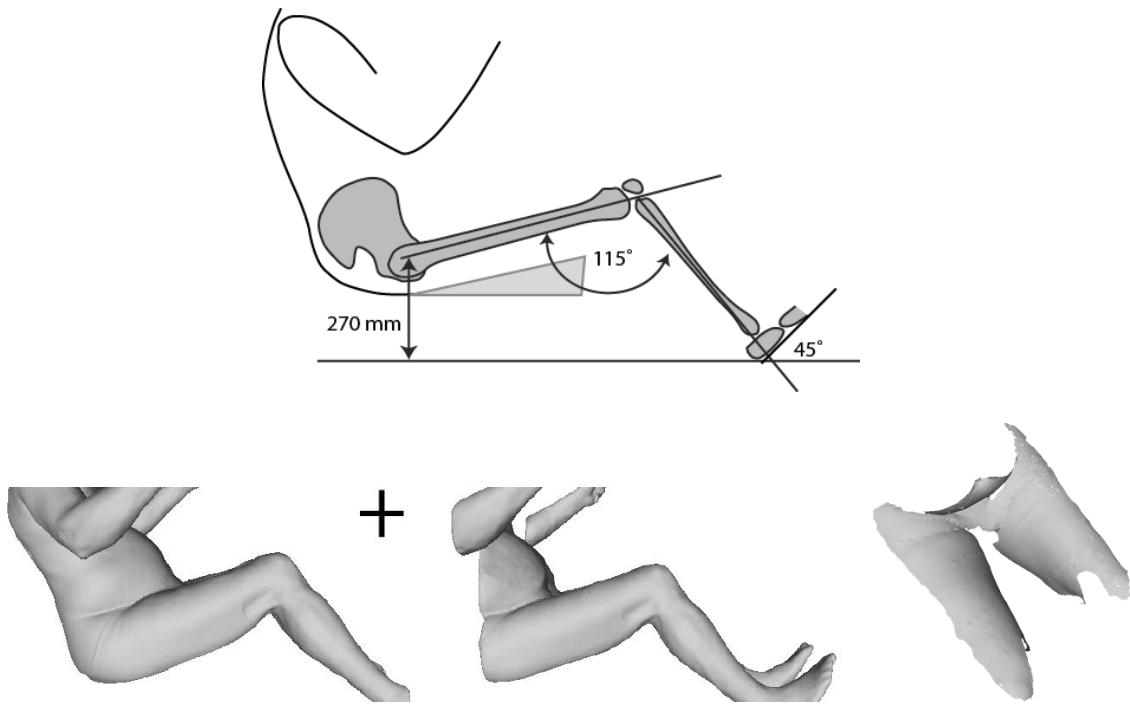


Figure C19. Illustration of the components of the automotive posture brought together into a single surface model.

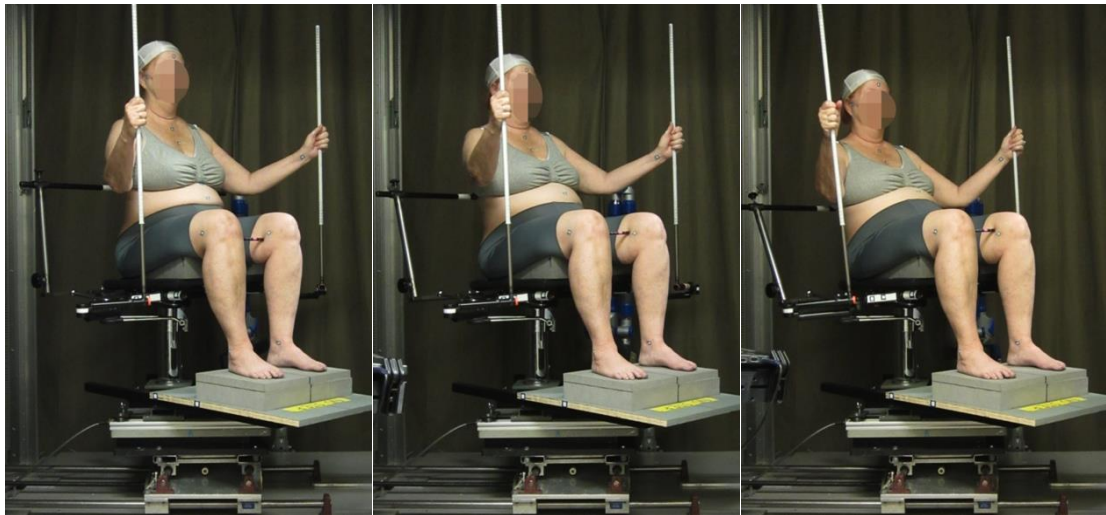


Figure C20. Example of person in recline postures

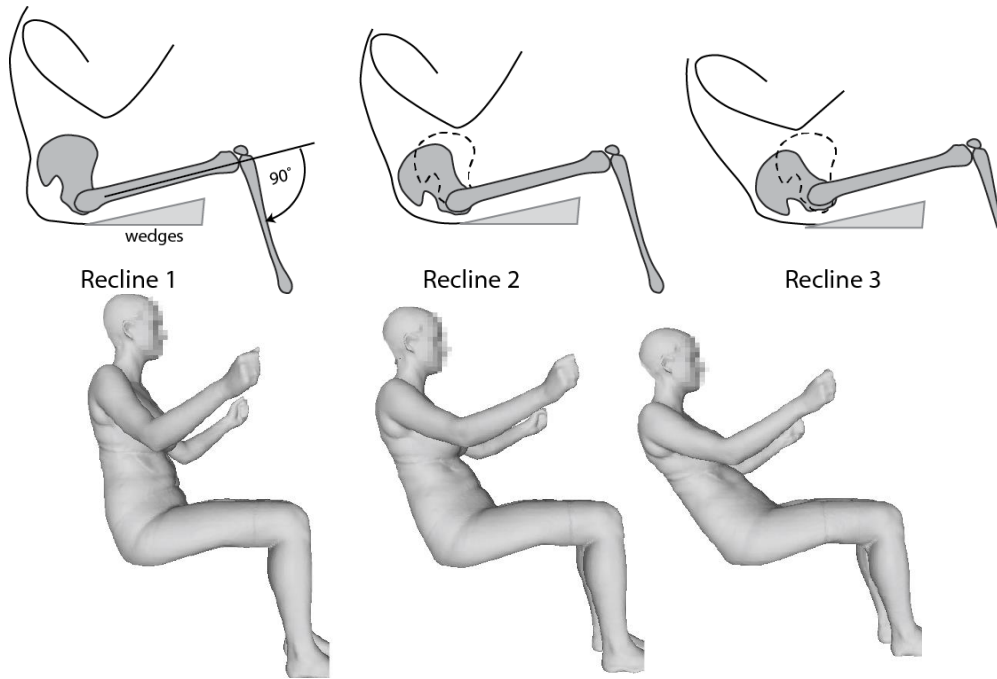


Figure C21. Recline postures 1 through 3 (left to right)

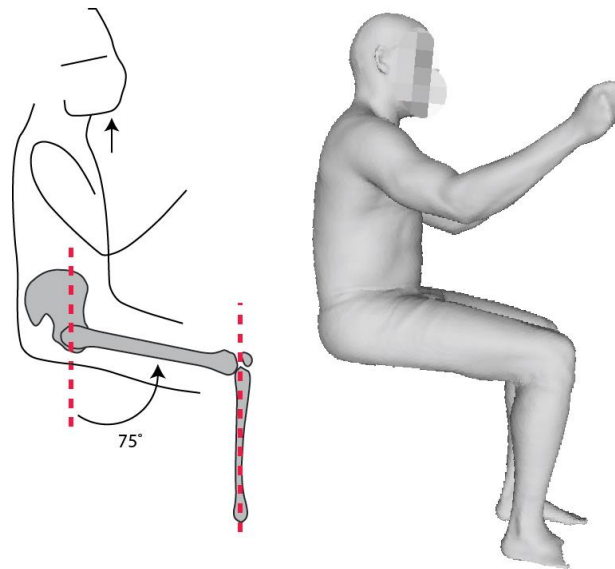


Figure C22. Sitting "L1" posture

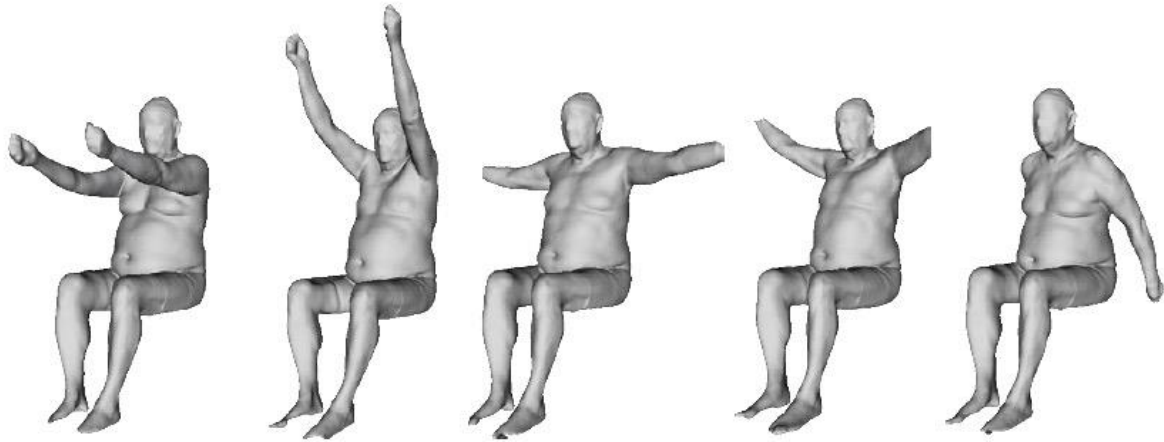


Figure C23. Shoulder range of motion: 90° flexion, maximum flexion, 90° abduction, maximum abduction and maximum extension (left to right)

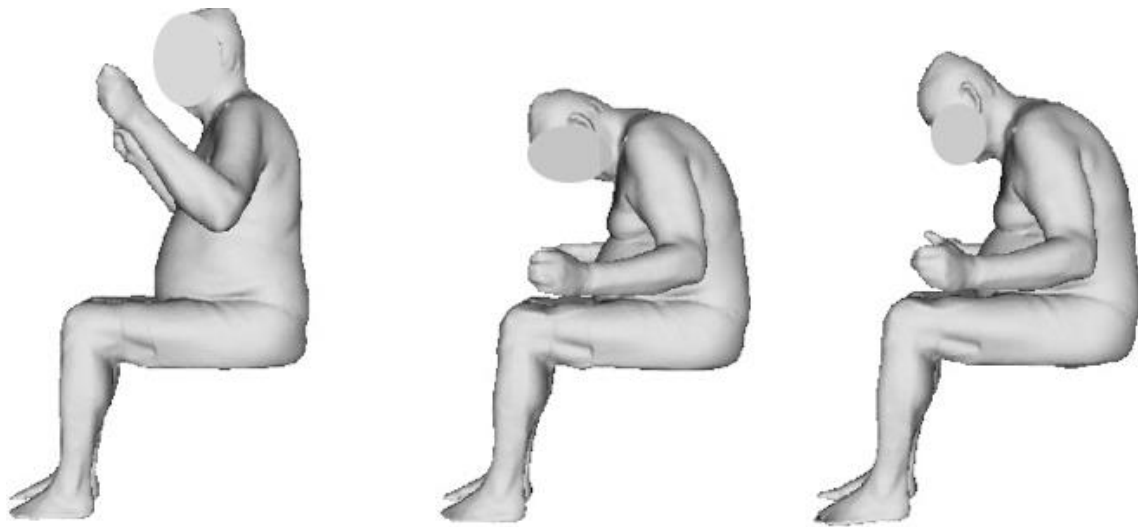


Figure C24. Spine Flexion at minimum, maximum and mid (left to right)

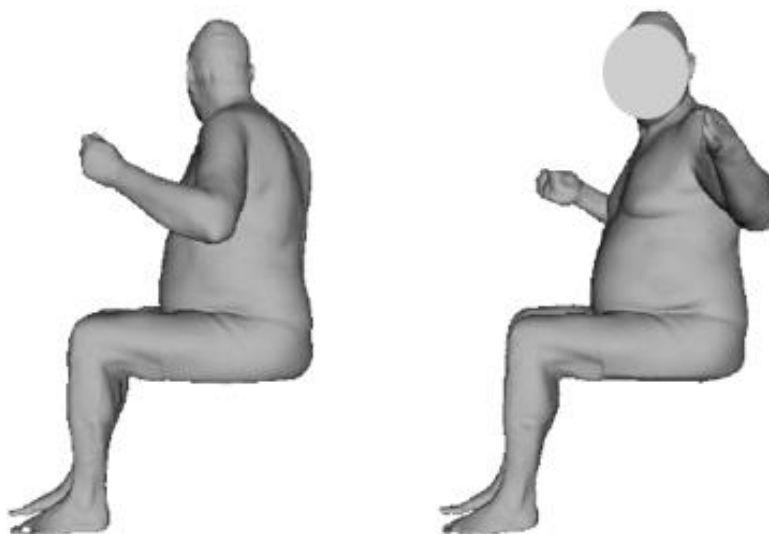


Figure C25. Spine rotation to the right and left



Figure C26. Hip flexion at maximum angle (left) and at comfortable angle (right)

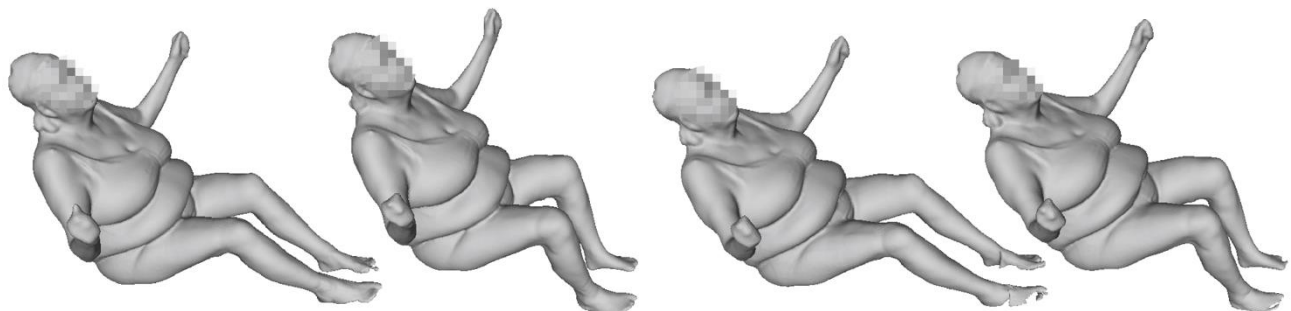


Figure C27. Medical sling postures with 0° back recline angle and knee angles at 60° and 90° (two on left) and with 20° back recline angle and knee angles at 60° and 90° (two on right)

Supine Scanning

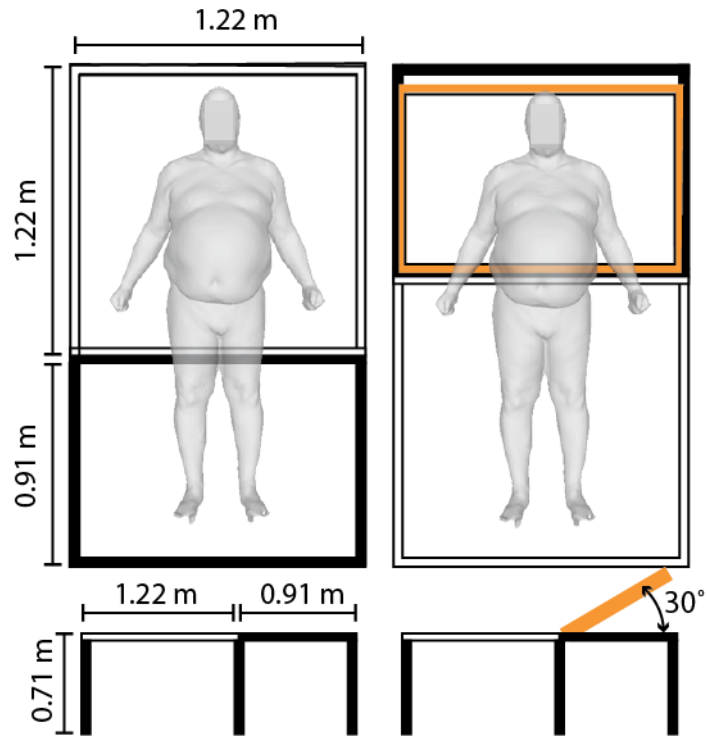


Figure C28. Dimensions of table used to record supine postures

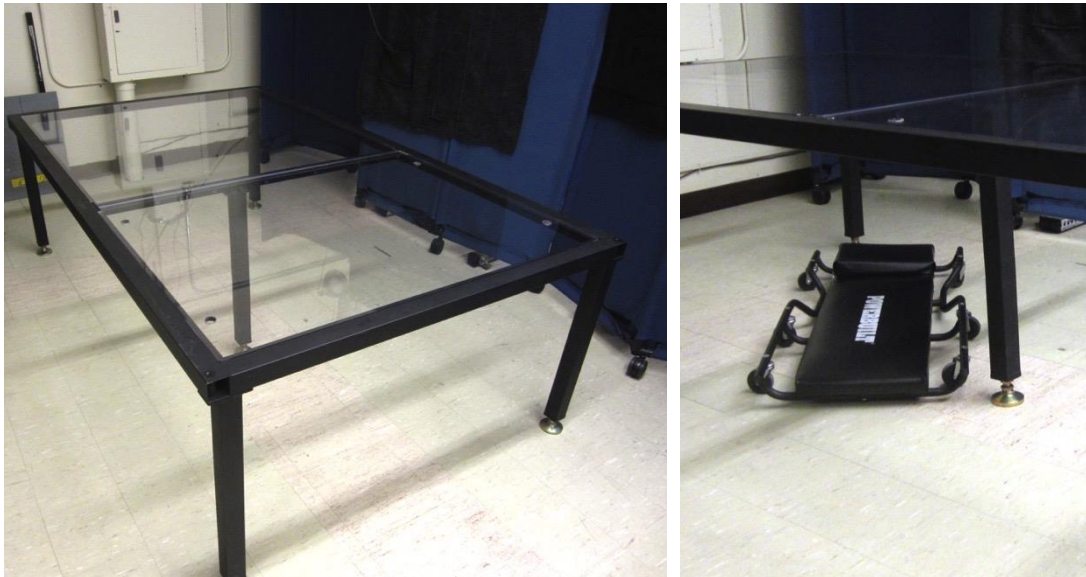


Figure C29. Photos of table used to record supine postures



Figure C30. Recording scanning supine posture with Artec and Sense scanners on participant's anterior (left) and posterior (right)

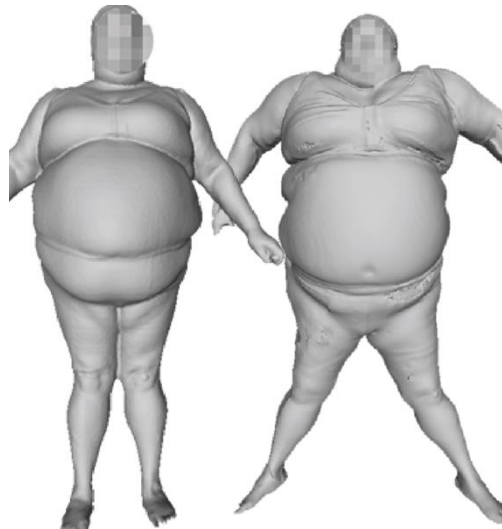
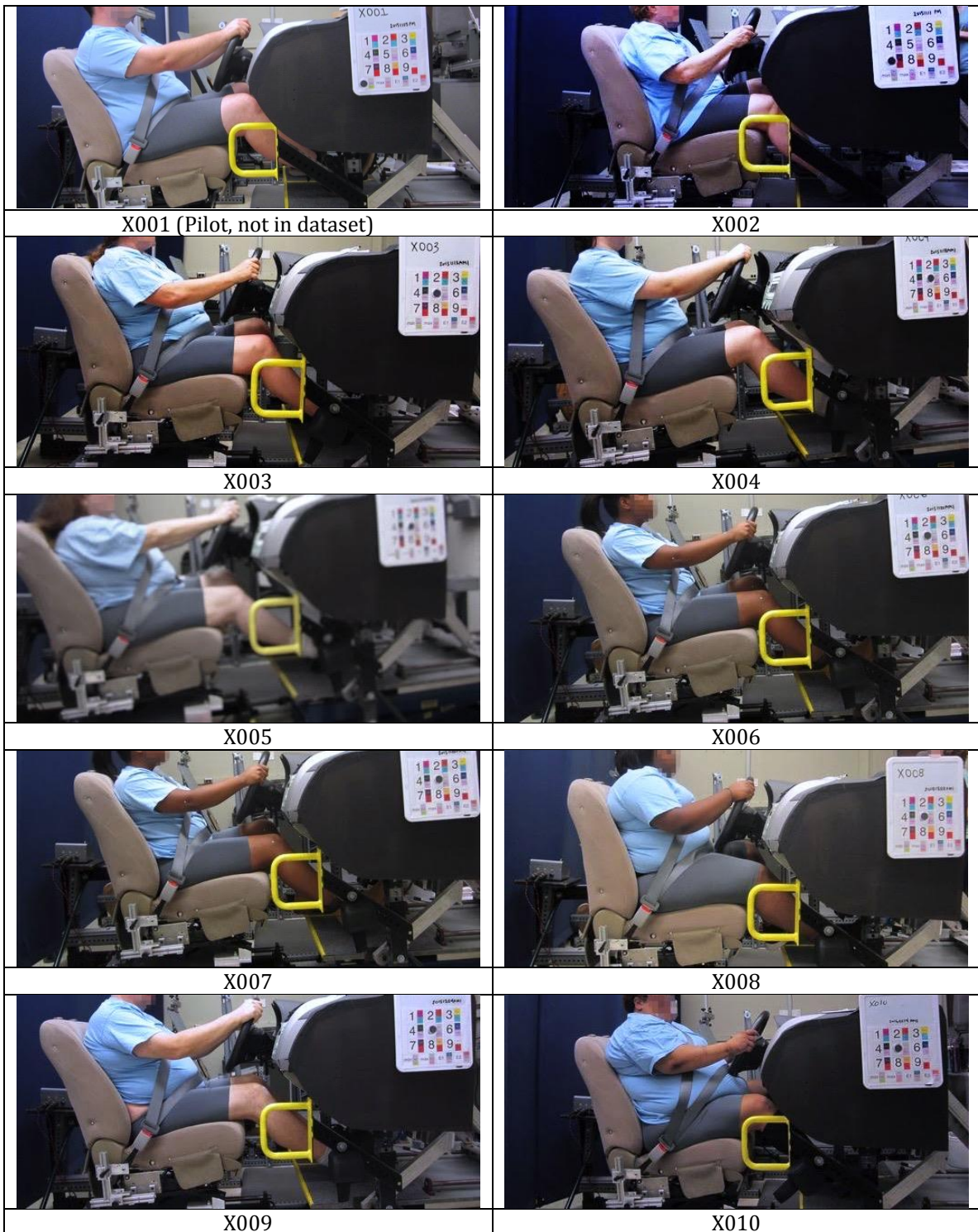
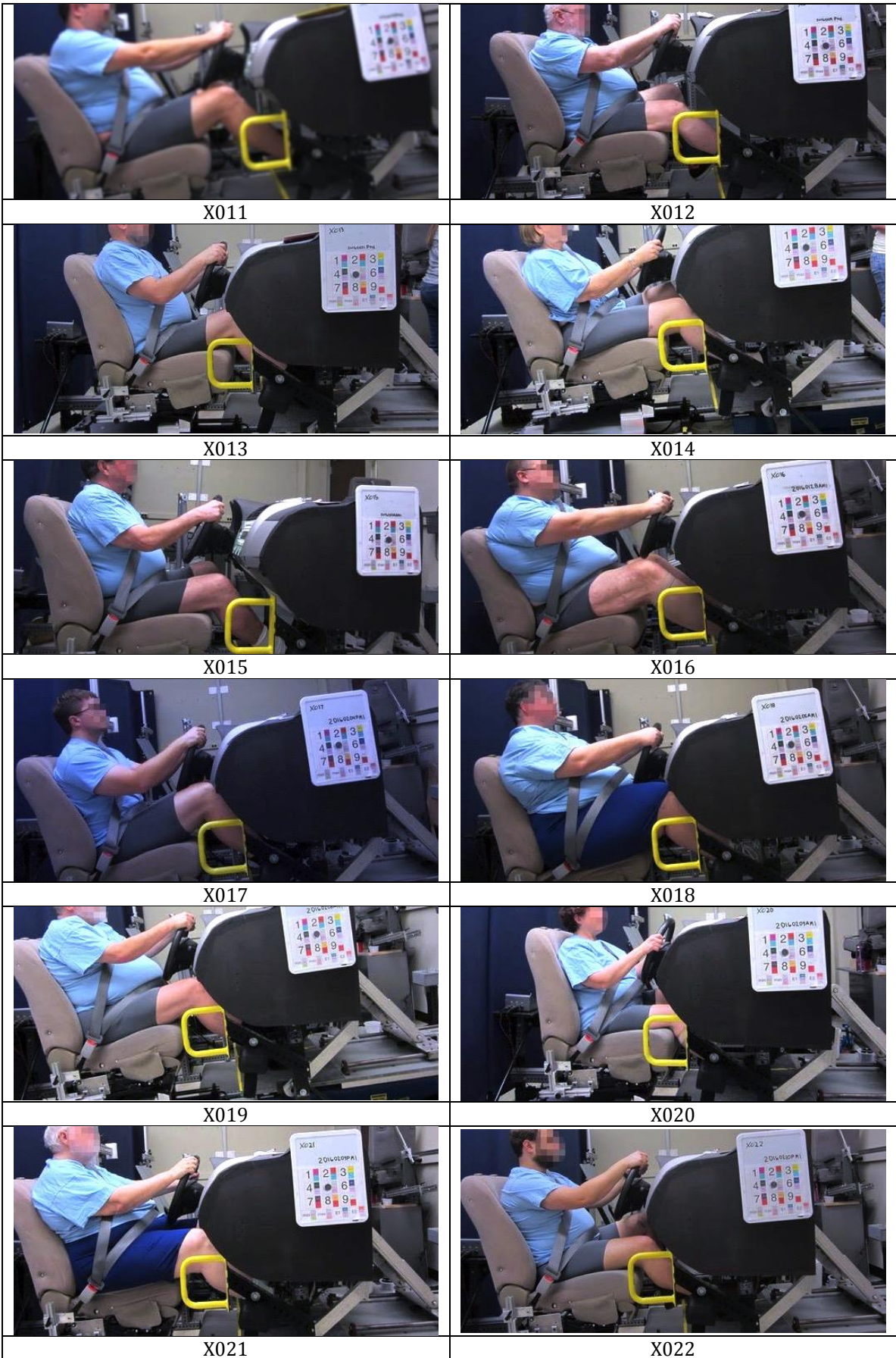
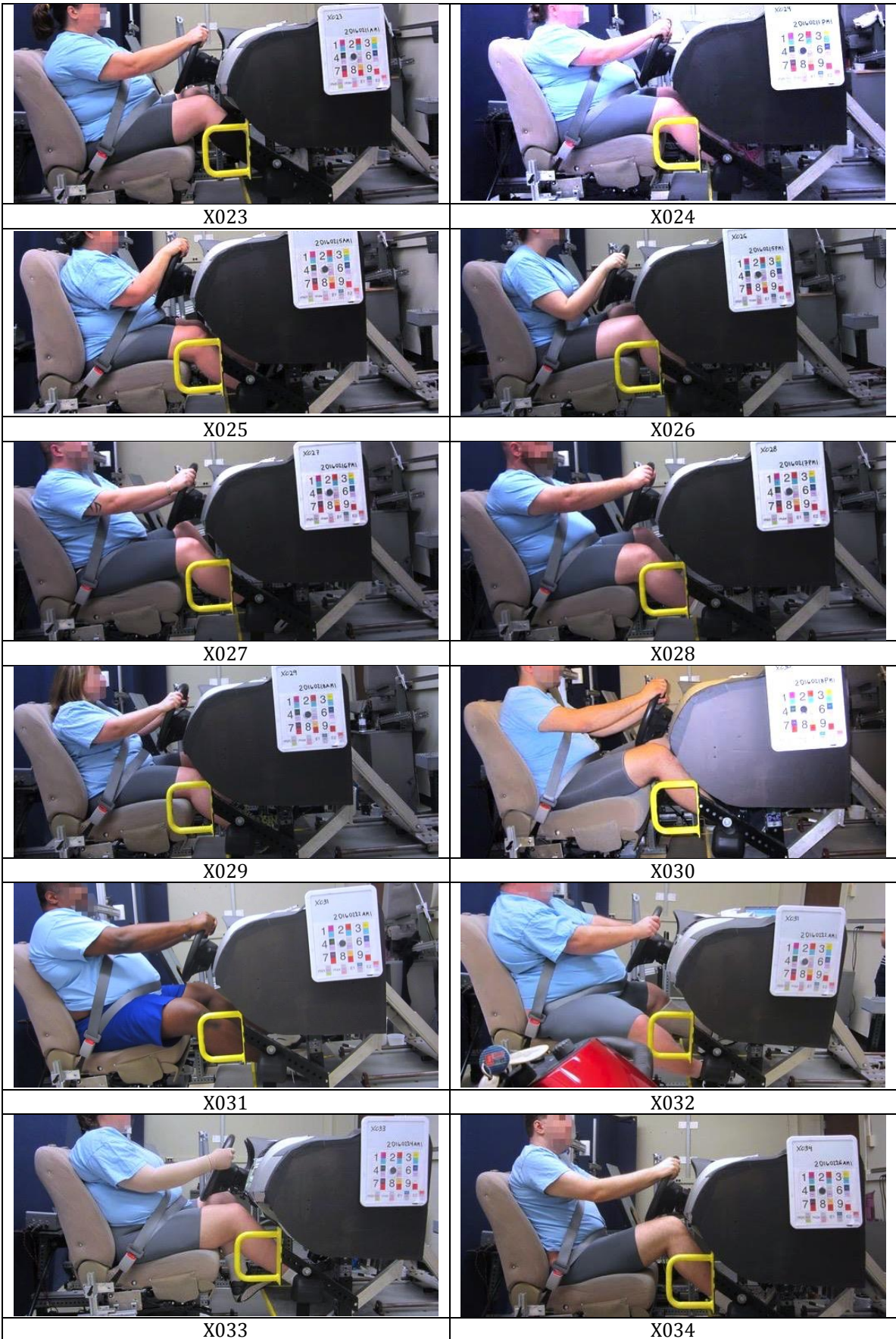


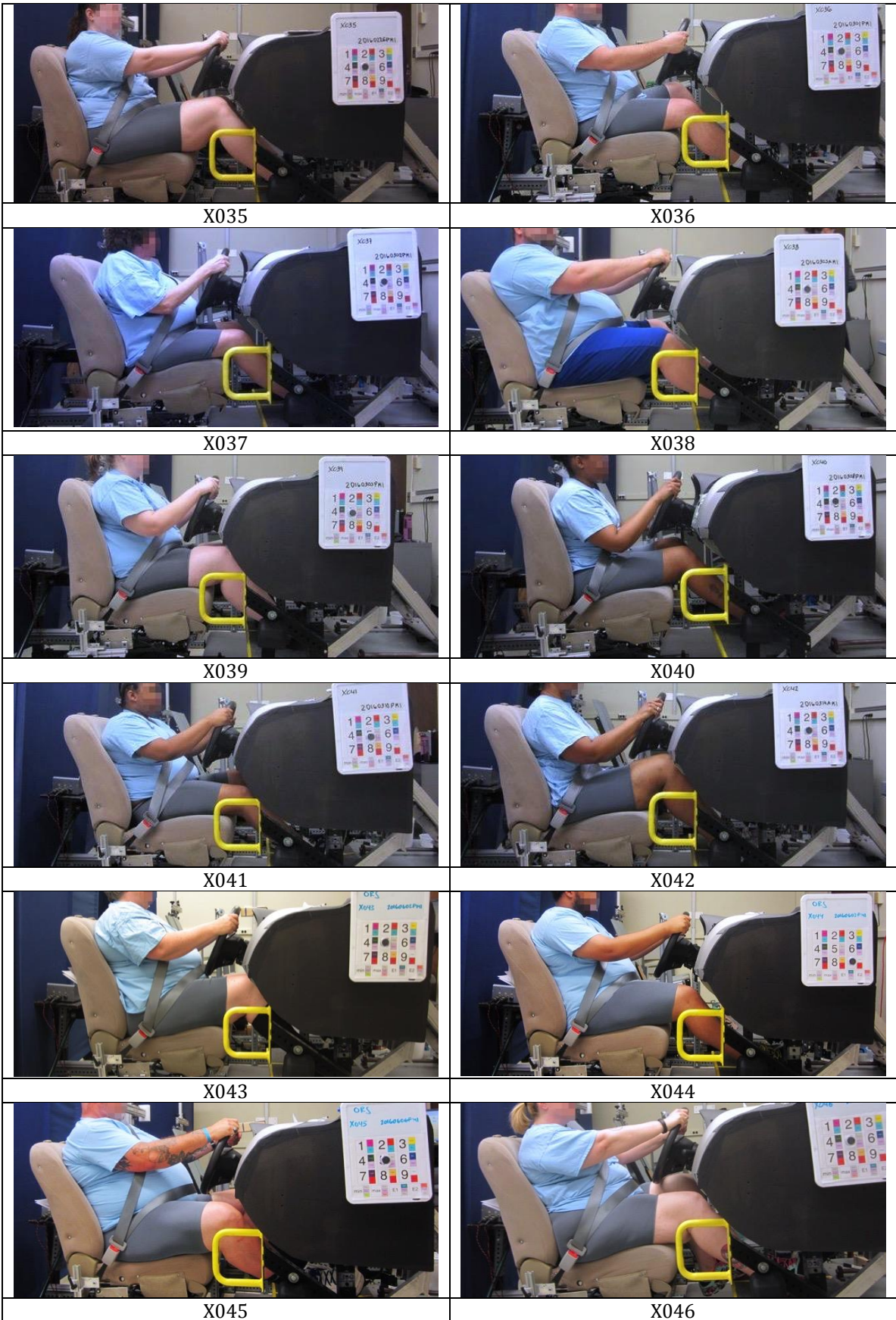
Figure C31. Standing (left) and supine (right) postures.




APPENDIX D. Individual Participant Belt Fit









	
X047 (did not test in mockup)	X048
	
X049	X050 (did not test in mockup)
	
X051	X052
	
X053	